Geochimica et Cosmochimica Acta 393 (2025) 107–121

Contents lists available at ScienceDirect

Geochimica et Cosmochimica Acta

journal homepage: www.elsevier.com/locate/gca

Effects of microbial alteration of oceanic crust on sulfur cycling in hydrothermal systems

Sarah N. Moriarty [a,*], Emma Bertran [b,c], James W. Dottin III [d,e], James Farquhar [d], David T. Johnston [b], Stephen J. Piercey [a], Dennis Sánchez-Mora [a], Michael G. Babechuk [a], Jason B. Sylvan [f], John W. Jamieson [a]

[a] Department of Earth Sciences, Memorial University of Newfoundland, St. John's, NL A1B 3X5, Canada
[b] Department of Earth and Planetary Sciences, Harvard University, Cambridge, MA 02138, United States
[c] ELSEVIER, RELX Group Publisher in Health & Medical Sciences, 1043 NX, Amsterdam, Netherlands
[d] Department of Geology, University of Maryland, College Park, MD 20742, United States
[e] Department of Earth, Environmental & Planetary Sciences, Brown University, Providence, RI 02912, United States
[f] Department of Oceanography, Texas A&M University, College Station, TX 77843, United States

ARTICLE INFO

Associate Editor: Esther Schwarzenbach

Keywords:
Sulfur Isotopes
Submarine Hydrothermal Systems
Seafloor Massive Sulfide Deposits
Mid-ocean Ridge
Microbial Sulfate Reduction

ABSTRACT

The accumulation of continental-derived sediment along mid-ocean ridges can influence sub-seafloor hydrothermal fluid circulation, including fluid composition, and the composition of associated mineral accumulations at the seafloor. The intermediate spreading-rate Juan de Fuca Ridge, off the west coast of North America, hosts both sedimented and sediment-free hydrothermal systems (Middle Valley and Axial Volcano, respectively), as well a hydrothermal system which occurs at the outer extent of continental-derived turbiditic sediment accumulation (Endeavour Hydrothermal Vent Field). The seafloor at Endeavour is mostly sediment-free and consists of basaltic lava flows. However, previously reported hydrothermal vent fluid compositions suggest the presence of buried sediment. Here, we compare S isotope ratios ($^{33}S/^{32}S$ and $^{34}S/^{32}S$) of hydrothermal chimney and talus samples, as well as sediments, from these three varyingly sedimented hydrothermal sites on the Juan de Fuca Ridge to S isotope ratios from hydrothermal deposits along the fast spreading archetypical East Pacific Rise in order to investigate the geological controls and microbial influence on hydrothermal S cycling. Using a combined isotopic mixing and fractionation model in $\Delta^{33}S$ and $\delta^{34}S$ space, we demonstrate that reduced S within sediments does not provide a significant contribution to the S budget of hydrothermal systems in sedimented environments on the Juan de Fuca Ridge. Instead, our data indicate that variations in S isotope compositions within and between vent fields reflects different degrees of sub-seafloor microbial crustal alteration and kinetic fractionations associated with reduction of seawater sulfate. The degree of microbially induced S isotope fractionation can be linked to intensity of crustal alteration and therefore age of the hydrothermal system. Our results illustrate the added value of a multiple S isotope approach to investigating S cycling in hydrothermal systems, and that the influence of microbial activity on hydrothermal systems extends well below the seafloor.

1. Introduction

Submarine hydrothermal systems and the associated formation of seafloor massive sulfide deposits at hydrothermal vents have been documented in all submarine tectonic settings, including fast- and slow-spreading mid-ocean ridges (MORs), and settings associated with subduction zones (Hannington et al., 2005). The composition of hydrothermal mineral deposits at the seafloor is controlled by a range of geologic variables including depth, substrate composition, presence of sediment at the seafloor, and magmatic volatile input (McDermott et al., 2015; Hannington et al., 2005; Monecke et al., 2014). Along MORs that are proximal to continental shelves, accumulation of turbidite deposits can result in hydrothermal circulation through not only the igneous crust, but also through 100s of m of terrigenous sediments (Davis et al., 1992; Davis and Fisher, 1994). Sub-seafloor mixing of locally infiltrated cold seawater with upwelling hydrothermal fluid can result in the

* Corresponding author.
E-mail address: snmoriarty@mun.ca (S.N. Moriarty).

https://doi.org/10.1016/j.gca.2024.11.031
Received 25 July 2024; Accepted 29 November 2024
Available online 5 December 2024

formation of an altered sediment reservoir cap, as well as a thermally insulated, permeable reservoir that promotes mineral precipitation below the seafloor (Davis et al., 1992; Davis and Fisher, 1994; Zierenberg et al., 1993; Zierenberg et al., 1998; Piercey, 2015). Hydrothermal vent fluids at sedimented ridges are generally lower temperature, higher pH, and more reducing than fluids from sediment-free ridges (Goodfellow and Zierenberg, 1997), resulting in mineral deposits at the seafloor that are rich in pyrrhotite and Fe-rich sphalerite (Ames et al., 1993; Zierenberg, 1994).

In addition to the formation of mineral deposits at the seafloor, submarine hydrothermal systems play a critical role in the cycling and exchange of S between the ocean and sub-seafloor (Shanks, 2001). Sub-seafloor fluid mixing, chemical exchange, and microbial processes result in changes in the S isotope compositions of the fluids and associated mineral deposits, and can be used to fingerprint specific geological and microbial processes associated with S cycling in submarine hydrothermal systems (e.g., Alt, 1995a; McDermott et al., 2015; Ohmoto, 1972; Ono et al., 2007; Shanks, 2001; Eickmann et al., 2014; Zierenberg, 1994). The specific geochemical and mineralogical characteristics of hydrothermal systems in sedimented environments suggest that hydrothermal S cycling may also be significantly different in these systems, relative to the more common hydrothermal systems in sediment-free environments (e.g., McDermott et al., 2015).

The measurement of S isotope ratios of sulfide and sulfate minerals in rock samples, as well as fluid samples collected from hydrothermal vents at the seafloor is a common tool for investigating S cycling in hydrothermal systems (e.g., Shanks et al., 1995; Shanks, 2001; Hannington et al., 2005; McDermott et al., 2015; Ono et al., 2007; Eickmann et al., 2014; Hughes et al, 2023; Peters et al., 2010; Peters et al., 2011). However, this tool is limited by the fact that mixing between different S reservoirs and isotope fractionation processes often result in non-unique isotopic signatures when relying only on traditional $^{34}S/^{32}S$ measurements, with these ratios expressed using standard delta (δ) notation and the Vienna-Canyon Diablo Troilite (V-CDT) reference:

$$\delta^{34}S = \left(\frac{^{34}R_{Sample}}{^{34}R_{V-CDT}} - 1\right) * 1000(‰) \quad (1)$$

where (^{34}R) represents $^{34}S/^{32}S$ (Beaudoin et al., 1994; Shanks et al., 1995). For example, the respective influences of reduced S (H_2S) derived from microbial sulfate reduction (MSR) and that of magmatic SO_2 disproportionation would both drive hydrothermal sulfide deposits at the seafloor to lower $\delta^{34}S$ values (Canfield, 2001; McDermott et al., 2015). Thus, the effectiveness of $\delta^{34}S$ alone for fingerprinting different mixing, chemical, and microbial processes associated with submarine hydrothermal systems is limited.

Measurements of the lower-abundance ^{33}S isotope (0.75% of total S) in addition to the more traditional higher abundance ^{34}S and ^{32}S isotopes (4.20% and 95.04% of total S, respectively; Ding et al., 2001) can partly overcome the limitation of non-unique isotopic signatures by recording small deviations in the mass-dependent isotope fractionation law (denoted as λ) associated with some kinetic and equilibrium fractionations (e.g., Farquhar et al., 2000; Johnston, 2011; Ono et al., 2007; McDermott et al., 2015). These deviations are quantified as $\Delta^{33}S$, which represents the difference between $\delta^{33}S$ values and expected $\delta^{33}S$ values assuming a mass law that approximated large low-temperature equilibrium fractionations:

$$\Delta^{33}S = \delta^{33}S - \left[\left(\frac{\delta^{34}S}{1000} + 1\right)^{0.515} - 1\right] * 1000(‰) \quad (2)$$

where 0.515 represents $^{33}\lambda$ for reference isotopic fractionation relationships (Farquhar and Wing, 2003). For mass-dependent isotopic fractionation processes, $^{33}\lambda$ can range from ~0.505 to 0.520 for different equilibrium and kinetic processes, leading to non-zero $\Delta^{33}S$ values (Farquhar et al., 2003; Farquhar et al., 2007; Johnston, 2011; Eldridge et al., 2016). For biological processes such as MSR, these variations can arise because of different biological pathways for intermediate S species in multi-step metabolic processes (Farquhar et al., 2003; Johnston et al., 2005; Ono et al., 2006).

Sulfur in hydrothermal fluids at MORs is sourced primarily from a combination of oceanic rocks of crustal and sub-crustal origin (i.e., basalt and/or peridotite) and seawater sulfate, with the possible contribution of minor S from magmatic volatiles, although direct magmatic input is more commonly associated with subduction related environments (Hannington and Scott, 1988; Yang and Scott, 1996; 2002). These primary S sources can additionally be modified by sub-seafloor microbial isotopic fractionation processes, which are thought to be more prevalent in sedimented environments (e.g., McDermott et al., 2015). The reduced S in unaltered oceanic crustal rocks generally has $\delta^{34}S$ and $\Delta^{33}S$ values of near 0‰ (Alt et al., 1989; Labidi et al., 2012; Labidi et al., 2014; Ono et al., 2012; Peters et al., 2010; Sakai et al., 1982; Sakai et al., 1984). Seawater sulfate has a well-constrained S isotopic value of $\delta^{34}S = 21‰$, and a $\Delta^{33}S = \sim 0.05‰$ (Tostevin et al., 2014; Johnston et al., 2014; Jaeschke et al., 2014; Eickmann et al., 2014; Ono et al., 2012). As seawater infiltrates downward beneath the seafloor at sediment-starved MORs and temperatures increase, the dissolved sulfate either precipitates as anhydrite or is thermochemically reduced through water–rock reactions (Shanks et al., 1981; Alt et al., 1989; Machel et al., 1995; Elderfield et al., 1999; Hughes et al., 2023). Progressive heating and leaching of reduced S from the host rocks thus results in an ascending hydrothermal fluid with a $\delta^{34}S$ signature that is widely modeled as reflective of simple two-component mixing between leached crustal S and seawater sulfate (Shanks, 2001; Alt, 1995a).

A two-component mixing model for S cycling cannot account for additional complexity in S cycling in hydrothermal systems as it does not adequately consider fractionation processes that can change the isotopic composition of the source reservoirs and fluids during hydrothermal circulation, such as microbial activity (Shanks, 2001). Sulfate-reducing microbes preferentially metabolize lighter isotopes, producing isotopically light reduced S products with $\delta^{34}S$ values commonly as low as −50‰ from initial seawater sulfate in the marine environment (Canfield, 2001; Rouxel et al., 2008; Peters et al., 2010; Peters et al., 2011; Halevy et al., 2023). At MORs near continental shelves, turbiditic sediments containing allochthonous organic carbon can support partial reduction of sulfate to H_2S via heterotrophic MSR (Frank et al., 2013; Ran and Simoneit, 1994; Shanks et al., 1995). Chemolithoautotrophic MSR can similarly affect igneous substrates in non-sediment bearing environments during low-temperature alteration of basalt (e.g., Bach and Edwards, 2003; Cowen et al., 2003; Edwards et al., 2003; Ono et al., 2012; Alt, 1995b; Rouxel et al., 2008). In this study, we employ measurements of multiple S isotope ratios of rock and sediment samples collected from the seafloor to identify different chemical and microbial processes associated with hydrothermal S cycling in areas with varying influence of continental sediments along the Juan de Fuca Ridge in the northeast Pacific Ocean. The S isotope data from the Juan de Fuca Ridge are also compared to S isotope data of sulfide samples from hydrothermal deposits hosted along the 9-10°N segment of the East Pacific Rise (EPR). The EPR is a fast-spreading MOR in the eastern Pacific Ocean that represents a potential endmember sediment-free geological setting to which the Juan de Fuca data can be compared.

2. Geological setting

The Juan de Fuca Ridge (Fig. 1), located off the coast of Vancouver Island and the Pacific Northwest, is a 490 km-long intermediate-rate (full spreading rate ~6 cm/yr) MOR separating the Juan de Fuca and Pacific plates (Davis et al., 1987). The Juan de Fuca Ridge hosts several hydrothermal systems with geologically-distinct settings. The Middle Valley vent field is located along the ~2460 m-deep, ~50 km-long, ~15 km-wide Middle Valley segment, a relict oceanic spreading center located on the northernmost part of the Juan de Fuca Ridge (Cruse et al., 2008; Goodfellow and Franklin, 1993; Ames et al., 1993). Middle Valley

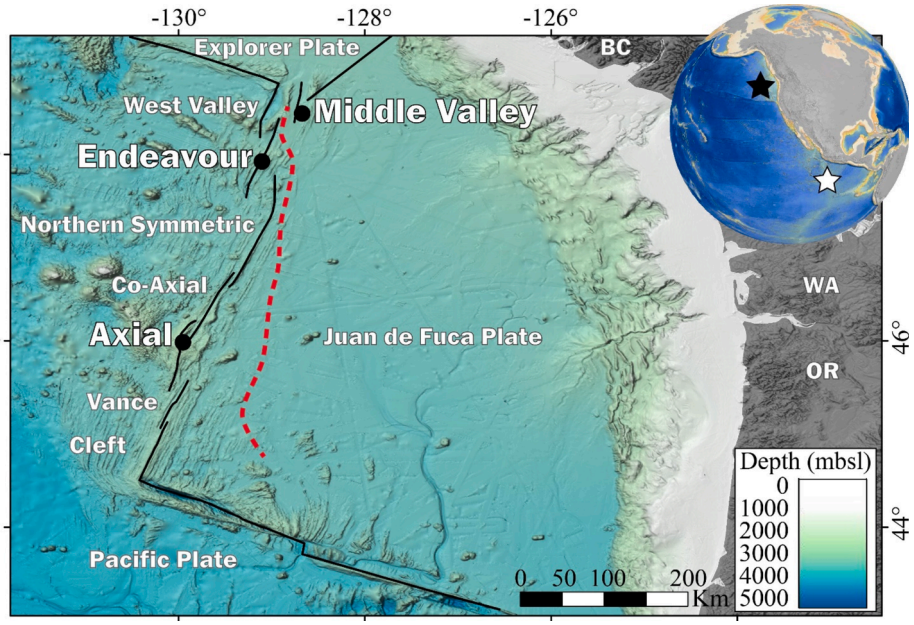

Fig. 1. Map showing segmentation of the Juan de Fuca Ridge and ridge bounding faults (black lines), major sites analyzed in this study (black dots), as well as global positions of the Juan de Fuca Ridge (black star), and 9-10°N EPR (white star). Bathymetry is from the Global Multi-Resolution Topography (GMRT) synthesis data set (Ryan et al., 2009). The dashed red line represents estimated extent of continent-derived turbiditic sediment cover based on global models (Divins, 2003), visual bathymetric smoothness, and known seafloor observations (modified from Van Ark et al., 2007; Cousens et al., 2002; Golden et al., 2003).

is infilled with up to 2 km of continental-derived turbiditic sediment (Davis and Villinger, 1992). The vent field includes Bent Hill, which is one of the largest known seafloor massive sulfide deposits on the modern ocean floor (Davis and Villinger, 1992; Zierenberg et al., 1998). Axial Volcano is a ~1500 m-deep active hotspot volcano located at the intersection of the southern Juan de Fuca Ridge and the Cobb-Eickelberg Seamount Chain. Axial volcano is situated distal to the continental shelf, and therefore out of reach of the turbiditic sediments that accumulate at Middle Valley. The volcano hosts several sites of high-temperature venting within its caldera (Chadwick et al., 2005; Clague et al., 2018; Hannington et al., 2005; Embley et al., 1990). All hydrothermal samples analyzed for this study were collected from a cluster of vents known as the International District, located along a fissure system on the southeastern part of the caldera (Kelley et al., 2014). The Endeavour vent field, situated between Axial volcano and Middle Valley, is hosted within the axial valley of the 90 km-long Endeavour Segment of the Juan de Fuca Ridge and is the location of Canada's first Marine Protected Area. The vent field is located at a depth of ~2050 m, and extends over 10 km of a basaltic substrate that has been hypothesized to have erupted onto previously deposited turbiditic sediments (Lilley et al., 1993; You et al., 1994; Kelley et al., 2012; Seyfried et al., 2003). Most of the documented high-temperature hydrothermal activity at Endeavour occurs at five main active vent clusters (listed from north to south): Sasquatch, Salty Dawg, High Rise, Main Endeavour (MEF), and Mothra (Fig. 2; Kelley et al., 2012).

Hydrothermal sulfide samples were also collected from three vent sites within the hydrothermal vent field at EPR 9-10°N (Biovent, Mosh Pit, and Lucky's Mound) to provide a comparative endmember for two-component mixing between S sourced from basalt and reduced seawater sulfate (Hannington et al., 2005; Shanks et al., 1995; Kelley et al., 2012; Perfit et al., 2012; Achberger et al., 2024). The region of the EPR between ~8°N and 11°N represents an archetypical sediment-free fast-spreading MOR and is commonly used as a baseline of comparison for hydrothermally active spreading centers in different tectonic settings (e.g., Kelley et al., 2012; Fornari et al., 2012).

3. Analytical methods

3.1. Sample collection

Sample collection was completed using the remotely operated vehicles *ROPOS, Doc Ricketts, Jason,* and the *Alvin* submersible over the course of several research cruises to the Juan de Fuca Ridge and 9-10°N EPR: AT15-36 (*R/V Atlantis*, 2008), AT15-47 (*R/V Atlantis*, 2009), MBARI *Western Flyer* (2011), *CCGS Tully* (2016), KM1812 (*R/V Kilo Moana*, 2018), and AT42-21 Atlantis (*R/V Atlantis,* 2019–2020). Hydrothermal rock samples were collected from either actively-venting or now-inactive high-temperature chimneys, or loose talus at the base of chimneys using robotic manipulator arms on the deep-sea vehicle (Fig. 2). Samples were selected for analysis based on high sulfide mineral abundance and to maximize spatial distribution of samples. The samples are composed primarily of a typical high-temperature sulfide-sulfate mineral suite with variable amounts of pyrite, chalcopyrite, sphalerite/wurtzite, marcasite, pyrrhotite, anhydrite, and barite and minor amorphous silica. Mineral distributions within the samples are often concentrically zoned, and generally follow typical temperature-solubility relationships, with higher-temperature minerals such as chalcopyrite and pyrrhotite concentrated in sample interiors, and pyrite/marcasite, sphalerite and barite towards the exteriors (e.g. Hannington et al., 1995). In many cases, patterns of mineral overprinting and multiple fluid conduits within samples indicate a complex evolution of hydrothermal flow within the chimneys. Anhydrite is only present in samples collected from actively-venting structures. Sediment samples were collected using 12-inch-long, 2.5-inch-diameter push cores from both on-axis, as well as 2 km off axis at Endeavour (Fig. 2).

3.2. Sample preparation

For rock samples, mineral-specific sub-samples were physically separated from the whole rock samples under a stereomicroscope using fine point forceps (Fig. 3). Mineral purities were visually estimated to be >80%. Impurities for the sulfide minerals generally consisted of primary and secondary silicates (i.e., amorphous silica, prehnite, etc..), co-precipitated mixed sulfide, and iron oxide material, while impurities

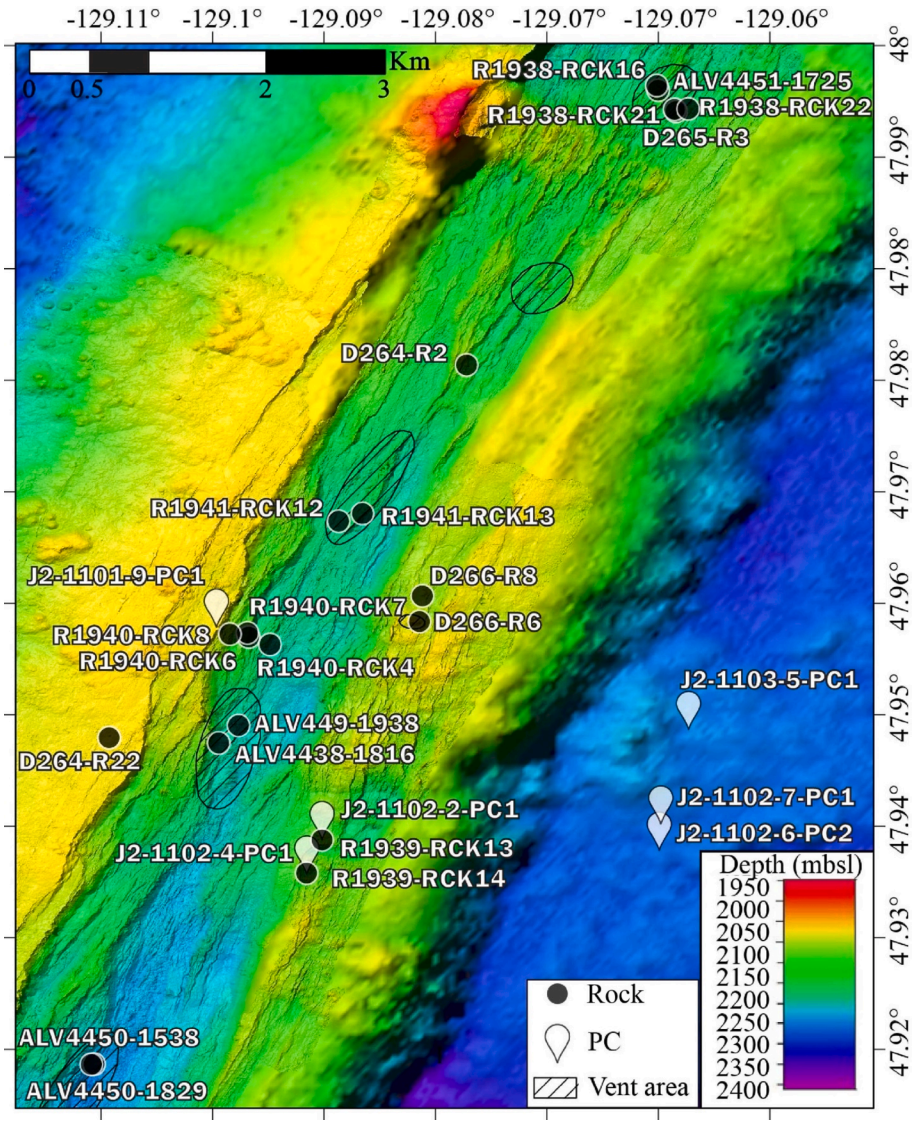

Fig. 2. Map of location of hydrothermal sulfide/sulfate (Rock) and sediment (PC) samples from the Endeavour segment used in this study. The five major active vent clusters at Endeavour (from north to south: Sasquatch, Salty Dawg, High Rise, MEF, and Mothra), as well as Zephyr Mound (under sample D266-R6) are denoted by hatch marks. Bathymetry is high resolution 2 m autonomous underwater vehicle-derived multibeam sonar bathymetry from Clague and Caress (2015) overlaid on top of 30 m ship-based multibeam sonar bathymetry from Kelley et al. (2015).

for the sulfate minerals were generally silicate minerals. Sulfide oxidation at low temperatures typically results in oxidation products with the same $\delta^{34}S$ values as the original reduced material (Shanks et al., 1995), but the effects of post-sampling oxidation on $\delta^{33}S$ values have not yet been fully investigated. Therefore, the sulfide sub-samples were placed into 6.0 M hydrochloric acid (HCl) for 24 hours at room temperature (~20 °C) to remove potential products of post-sampling sulfide oxidation, after which they were tripled rinsed with ethanol and stored in an airtight container.

For the sediment cores, internal stratigraphy was not preserved during sampling, preventing discrete sampling at specific depths within the core. However, loose sediment subsamples were collected from bottom layers below the redox boundary, where present. The sediment samples (Fig. 4) were kept frozen (<-18 °C) post-collection in an effort to minimize oxidation, then oven dried at ~50 °C. The dried sediments were bulk analysed and not treated with HCl prior to reduction for isotopic analysis. The sediment samples were classified based on visually estimated relative abundances of unaltered basalt clasts, plume fallout (i.e., unlithified sulfide grains), and turbiditic/pelagic sediment content. Samples J2-1101–9-PC1, J2-1102–6-PC2, and J2-1102–7-PC1 all have visible basalt clasts comprising >2% of the sample. Samples J2-1102–2-PC1 and J2-1102–4-PC1 are reddish in colour, indicating an oxidized hydrothermal component. Sulfide crystals with secondary Fe-oxyhydroxide coatings were visible under stereomicroscope. Sample J2-1103–5-PC1 consists of nearly entirely turbiditic/pelagic sediment, with <1% visible basalt clasts under stereomicroscope, and no visible sulfide material.

3.3. Isotopic measurements

Isotopic analyses were conducted at two laboratories: The Gas Source Mass Spectrometry I Laboratory at the University of Maryland, College Park (UMD), and the Johnston Laboratory at Harvard University, in Cambridge, MA. Both the sulfide separates (pyrite, pyrrhotite, wurtzite, marcasite, and chalcopyrite) and bulk sulfide from the sediments were converted to silver sulfide (Ag_2S) via chromium reduction (Canfield et al., 1986). Sulfate in anhydrite and barite was converted to Ag_2S using the Thode solution procedure described in Thode et al. (1961) and Forrest and Newman (1977). The product Ag_2S was then transferred to a Ni pressurized bomb reaction vessel and heated

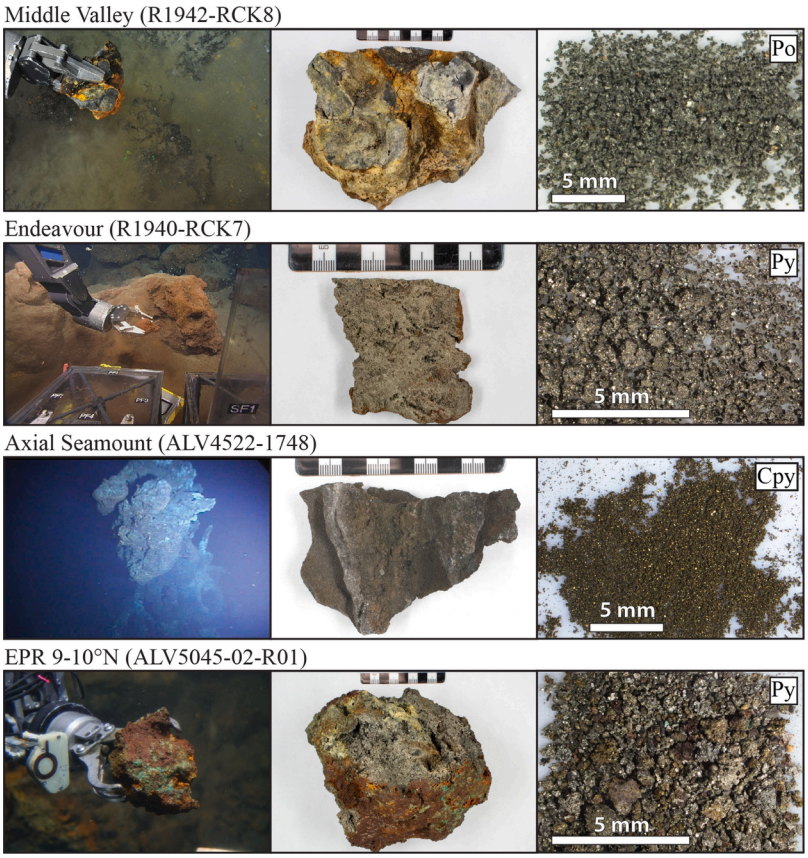

Fig. 3. Examples of rock samples collected from the four hydrothermal vent sites in this study, showing sampling location at the seafloor (left panel), hand sample (centre panel), and mineral separates prepared for isotopic analysis (right panel).

overnight at 250 ℃ in a fluorine gas atmosphere to generate SF_6 gas.

The generated SF_6 was purified using cryogenic techniques and gas chromatography to reduce residual contaminants produced during the fluorination process (e.g., HF). The purified SF_6 was then introduced into a dual-inlet ThermoFinnigan MAT 253 gas source mass spectrometer to measure the concurrent ionic beams of $^{32}SF_5^+$, $^{33}SF_5^+$, and $^{34}SF_5^+$ and the corresponding masses: 127, 128 and 129 Da, respectively. The isotopic ratios for $^{33}S/^{32}S$ and $^{34}S/^{32}S$ are reported relative to the Vienna-Canyon Diablo Troilite (V-CDT) reference scale. This scale utilizes the definition of artificial silver sulfide material IAEA S-1, which has a defined $\delta^{34}S$ value of −0.3‰ (Coplen and Krouse, 1998). However, there is no defined $\delta^{33}S$ value for IAEA S-1. For this study we use −0.055‰ as the $\delta^{33}S$ value for IAEA S-1 (Ono et al., 2007). Calculated analytical uncertainties were determined by repeat analyses of standards IAEA S-1 versus the internal reference gas. Intra-laboratory reproducibility (1σ) for UMD samples is ±0.2‰ and ±0.008‰ for $\delta^{34}S$ and $\Delta^{33}S$, respectively (Wu et al., 2018). Intra-laboratory reproducibility (1σ) for analyses performed at Harvard is reported as ±0.2‰ and ±0.006‰ for $\delta^{34}S$ and $\Delta^{33}S$, respectively (Masterson, 2016).

4. Results

Overall, $\delta^{34}S$ values for sulfide, sulfate, and bulk sediment samples from all sites in this study range from 0.4‰ to 7.5‰, 18.8‰ to 22.1‰, −18.8‰ to 3.6‰, respectively. Corresponding $\Delta^{33}S$ values for sulfide, sulfate, and bulk sediment samples from all sites in this study range from −0.147‰ to 0.043‰, 0.008‰ to 0.052‰, and −0.019‰ to 0.024‰, respectively (Fig. 5). Sulfur isotope ratios of sulfide mineral samples from Middle Valley (n = 3) range from 6.2‰ to 7.5‰, and −0.014‰ to −0.147‰ for $\delta^{34}S$ and $\Delta^{33}S$, respectively. The S isotope ratios from Endeavour sulfide mineral samples (n = 18) are more variable, ranging from 0.4‰ to 5.4‰ for $\delta^{34}S$, and −0.028‰ to 0.061‰ for $\Delta^{33}S$. Sulfide mineral samples from Axial Volcano (n = 2) have $\delta^{34}S$ values of 3.2‰ and 4.6‰, and $\Delta^{33}S$ values of −0.024‰ and −0.066‰. Sulfide mineral samples from EPR (n = 3) have $\delta^{34}S$ values ranging from 3.2‰ to 5.9‰, and $\Delta^{33}S$ values from 0.023‰ to 0.043‰ (Table 1; Fig. 6). The $\delta^{34}S$ values of the sulfate mineral samples from all Juan de Fuca Ridge sites range from 18.8‰ to 22.1‰. The $\Delta^{33}S$ values for the sulfate mineral samples range from 0.008‰ to 0.052‰ (Table 2; Fig. 6). The plume fallout sediments (n = 2) have S isotope values ranging from 2.0‰ to 3.6‰ and −0.019‰ to 0.013‰ for $\delta^{34}S$ and $\Delta^{33}S$, respectively. The turbiditic/pelagic sediments with 10–20% basalt (n = 2) have S isotope values ranging from −3.4‰ to −2.1‰ and 0.004‰ to 0.013‰ for $\delta^{34}S$ and $\Delta^{33}S$, respectively. The turbiditic/pelagic sediments with negligible (<1–2%) basalt (n = 2) have S isotope values ranging from −18.8‰ to −17.9‰ and −0.006‰ to 0.024‰ for $\delta^{34}S$ and $\Delta^{33}S$, respectively (Table 3; Fig. 6).

5. Discussion

The $\delta^{34}S$ and $\Delta^{33}S$ values for hydrothermal deposits along both the Juan de Fuca Ridge and EPR 9-10°N reported in this study are consistent with the range of results reported from previous studies of modern submarine hydrothermal systems in all tectonic settings (i.e., generally ~ -25 to +25‰ for $\delta^{34}S$ [e.g., Hannington et al., 2005; Adshead, 1996; Peters et al., 2011; Aquino et al., 2022; Shanks and Bischoff, 1980, Zierenberg, 1994], and ±0.2‰ for $\Delta^{33}S$ [Peters et al., 2010; Peters et al., 2011; McDermott et al., 2015; Aoyama et al., 2014; Jaeschke et al.,

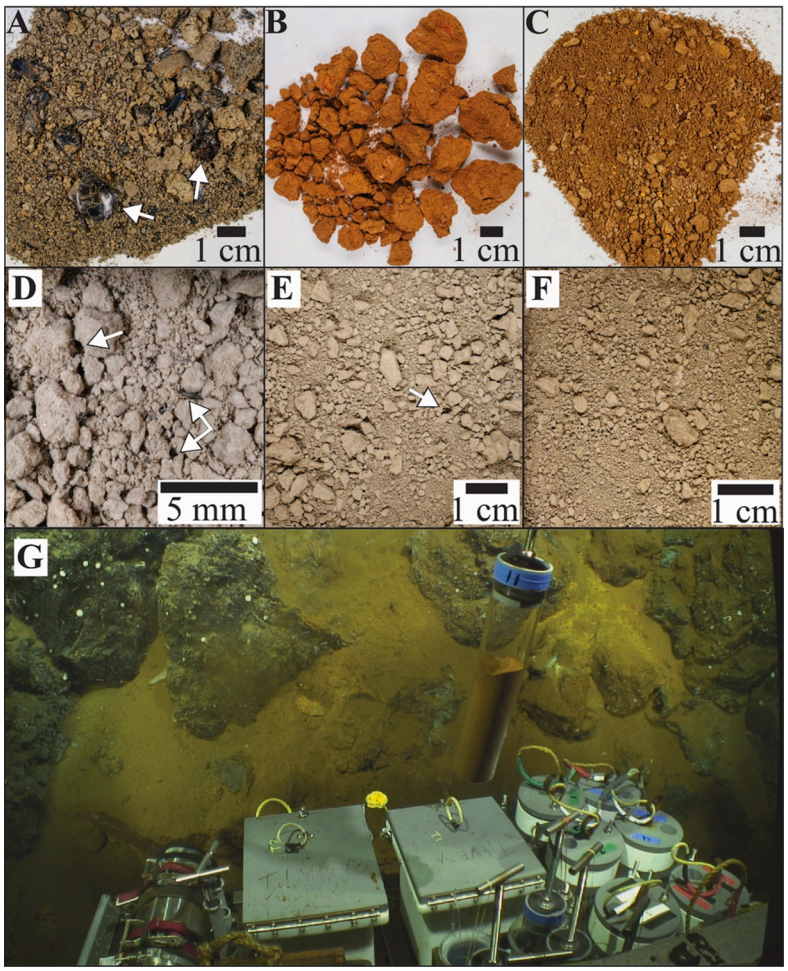

Fig. 4. Bulk sediments from Endeavour used for isotopic analysis: A) J2-1101–9-PC1, B) J2-1102–2-PC1, C) J2-1102–4-PC1, D) J2-1102–6-PC2, E) J2-1102–7-PC1, F) J2-1103–5-PC1, and G) example of sediment collection (J2-1102–2-PC1) on the seafloor. Arrows indicate examples of basalt clasts in samples where they are present.

2014; Eickmann et al., 2014; Ono et al., 2007]).

The results show a limited range of $\delta^{34}S$ within the different types of samples (sulfide, sulfate minerals, and sediment types) (Fig. 5a; Tables 1-3). The $\Delta^{33}S$ results, however, indicate a wider variability in isotopic compositions for the sulfide minerals that would not be detected if relying only on the more traditional $\delta^{34}S$ values (Fig. 5b). Across all four hydrothermal sites, spread over two MORs, the S isotope results for sulfide minerals in this study (Table 1) form a near vertical array in $\Delta^{33}S$ versus $\delta^{34}S$ space, indicating variability in $\Delta^{33}S$ coupled with the limited range in $\delta^{34}S$ (Figs. 5, 6). No major mineral-specific trends are apparent for the sulfide S isotope data (Fig. 6). However, the EPR samples all have positive $\Delta^{33}S$ values, whereas the Juan de Fuca Ridge samples are dominantly negative (Fig. 6).

5.1. Archetypical sediment-free fast-spreading ridges

The average $\delta^{34}S$ value of 4.1‰ (±0.2‰, 1σ, n = 3) for the sulfide-rich samples from the archetypical fast-spreading sediment-free EPR measured in this study falls within the typical range of $\delta^{34}S = \sim 1$ and 5‰ for EPR hydrothermal sulfide precipitates and sediment-free MORs (Hannington et al., 2005 and sources therein; Ono et al., 2007). This range in $\delta^{34}S$ values is traditionally interpreted to reflect the dominant control of two-component mixing between reduced S derived from the leaching of sulfide minerals in relatively fresh oceanic crust ($\delta^{34}S \approx 0$‰; Peters et al., 2010; Ono et al., 2012; Labidi et al., 2012) and a ~ 20–30% contribution from S derived from thermochemical reduction of seawater sulfate during fluid downwelling into the crust (Ono et al., 2007; Fig. 7). More recent reports of $\Delta^{33}S$ values in conjunction with the traditional $\delta^{34}S$ values from EPR 9-10°N, however, suggest that buffering of the ascending hydrothermal fluid S isotopic composition via isotopic exchange with anhydrite also modifies the isotopic composition of the hydrothermal precipitates by shifting to more positive $\Delta^{33}S$ values (i.e. the "anhydrite buffer" model; Fig. 7; Ohmoto et al., 1983; Ono et al., 2007). The average of $\Delta^{33}S$ values from the EPR samples measured in this study, 0.030‰ (±0.012‰, 1σ, n = 3), is consistent with the results from Ono et al. (2007) and suggests modification of the two-component mixing isotopic composition of the fluids by varying degrees of equilibration from anhydrite buffering at ~350 °C to 400 °C (Fig. 7). This temperature range is consistent with previously recorded fluid venting temperatures at EPR 9-10°N (maximum temperature 386 °C; Yucel and Luther, 2013). The absence of both negative $\delta^{34}S$ and $\Delta^{33}S$ values suggests that microbial processing of S is not an important process at this site, and the S isotope compositions of the precipitates is controlled by abiotic processes. The results from EPR 9-10°N can therefore be used as a baseline for comparison for the samples from the Juan de Fuca Ridge, for which the S isotope data suggest modification resulting from microbial processes in the sub-seafloor (see below).

5.2. Sediment-covered and mature, intermediate-rate spreading ridges

The sulfide minerals from the three hydrothermal sites along the variably sedimented intermediate-rate spreading Juan de Fuca Ridge

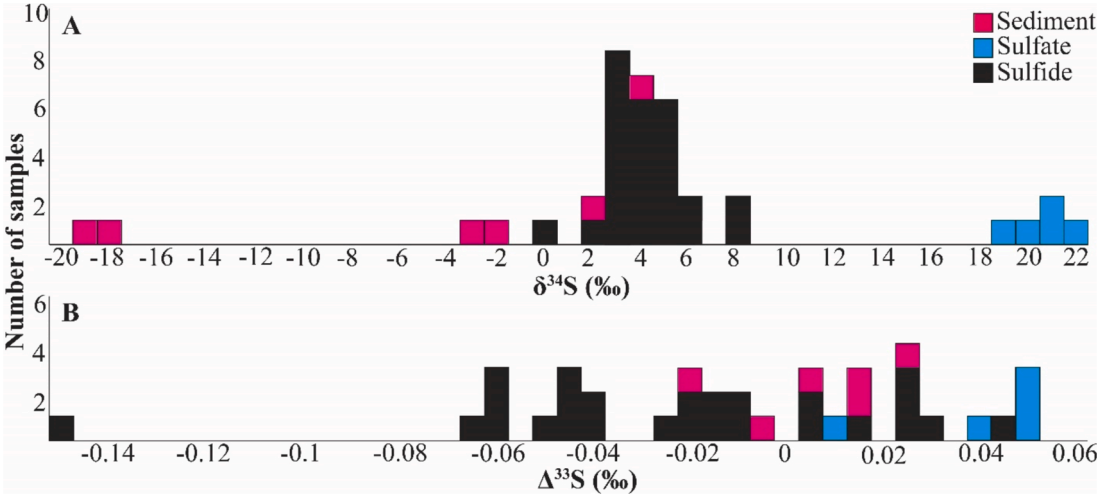

Fig. 5. Histograms showing result distribution for: (A) $\delta^{34}S$ values for sulfide, sulfate and sediment samples from the Juan de Fuca Ridge, and (B) corresponding $\Delta^{33}S$ values.

Table 1
Results of S isotope analyses of massive sulfide sample mineral separates from Juan de Fuca Ridge and 9-10°N EPR.

Sample	Location	Vent area	Mineral	$\delta^{34}S$ (‰)	±1σ (‰)	$\Delta^{33}S$ (‰)	±1σ (‰)
R1942-RCK8	Middle Valley	Bent Hill	Po	7.5	0.2	−0.147	0.006
R1942-RCK16	Middle Valley	Bent Hill	Po	7.5	0.2	−0.041	0.006
R1942-RCK10	Middle Valley	Bent Hill	Py	6.2	0.2	−0.062	0.006
D265-R3	Endeavour	Sasquatch	Py	4.8	0.2	−0.051	0.006
R1938-RCK16	Endeavour	Sasquatch	Py	2.5	0.2	0.003	0.008
R1938-RCK21	Endeavour	Sasquatch	Py	3.6	0.2	0.025	0.008
R1938-RCK22	Endeavour	Sasquatch	Po	4.7	0.2	−0.022	0.006
ALV4451-1725	Endeavour	Sasquatch	Wz	2.8	0.2	−0.022	0.006
D264-R2	Endeavour	Salty Dawg	Py	4.2	0.2	−0.012	0.006
R1941-RCK12	Endeavour	High Rise	Py	4.4	0.2	−0.044	0.006
R1941-RCK13	Endeavour	High Rise	Py	4.9	0.2	−0.015	0.006
D266-R6	Endeavour	Zephyr Mound	Cpy	3.1	0.2	−0.061	0.006
D266-R8	Endeavour	Zephyr Mound	Py	5.4	0.2	−0.058	0.006
ALV4438-1816	Endeavour	MEF	Cpy	4.1	0.2	−0.040	0.006
R1939-RCK14	Endeavour	MEF	Cpy	3.9	0.2	0.006	0.008
R1939-RCK13	Endeavour	MEF	Mrc	0.4	0.2	−0.010	0.006
ALV4449-1938	Endeavour	MEF	Po	1.5	0.2	0.028	0.008
R1940-RCK4	Endeavour	MEF	Py	3.2	0.2	−0.043	0.006
R1940-RCK6	Endeavour	MEF	Py	3.8	0.2	−0.043	0.006
R1940-RCK7	Endeavour	MEF	Py	5.2	0.2	−0.013	0.006
R1940-RCK8	Endeavour	MEF	Py	3.4	0.2	0.013	0.008
ALV4522-1748	Axial	International District	Cpy	4.6	0.2	−0.066	0.006
ALV4522-1725	Axial	International District	Py	3.2	0.2	−0.024	0.006
AL5044-06-R01	9-10°N EPR	Mosh Pit	Py	3.2	0.2	0.023	0.008
AL5045-02-R01	9-10°N EPR	Lucky's Mound	Py	5.9	0.2	0.023	0.008
AL5046-08-R01	9-10°N EPR	Biovent	Py	3.3	0.2	0.043	0.008

Py = pyrite, cpy = chalcopyrite, po = pyrrhotite, mrc = marcasite, wz = wurtzite.

show remarkably consistent $\delta^{34}S$ values between the different vent fields, similar to the EPR samples, despite the different geological settings of the vent fields (Fig. 8). Taken together, the sulfide minerals from the Axial (sediment-free) and Endeavour (potential buried sediment) sites also have similar $\delta^{34}S$ values, with an overall range between 0.4‰ to 5.4‰. The $\delta^{34}S$ values for sulfide minerals from hydrothermal deposits at Axial Volcano in this study are consistent with previous S isotope analyses of sulfide minerals from this site, where hydrothermal sulfide $\delta^{34}S$ values range from 2‰ to 9‰ (Hannington and Scott, 1988; Crowe and Valley, 1992). These high $\delta^{34}S$ values (relative to EPR) were previously attributed to localized TSR of seawater SO_4^{2-} at vent sites during deposit formation (Hannington and Scott, 1988). The Middle Valley $\delta^{34}S$ values are slightly more positive (range of 6.2‰ to 7.5‰) than the values for Axial and Endeavour. These values are consistent with previously published average Middle Valley data for surficial hydrothermal sulfide samples ($\delta^{34}S$ = 6.3‰; Goodfellow and Blaise, 1988; Stuart et al., 1994b; Duckworth et al., 1994; Goodfellow and Franklin, 1993) and dissolved H_2S (7.7‰; Cruse et al., 2008), and also consistent with a general trend of slightly higher $\delta^{34}S$ values at all sediment-hosted hydrothermal sites, relative to sediment-free MOR settings (Hannington et al., 2005). Similar to Axial, previously reported elevated $\delta^{34}S$ values for Middle Valley samples have been interpreted to indicate greater influence of locally reduced seawater SO_4^{2-} during hydrothermal fluid cycling relative to the archetypical EPR and most other sediment-free hydrothermal sites (e.g., Duckworth et al., 1994; Stuart et al., 1994a; Stuart et al., 1994b; Cruse et al., 2008; Goodfellow and Blaise, 1988; Goodfellow and Franklin, 1993). Previously collected subseafloor (non-hydrothermal) sediment cores from Middle Valley contain reduced S with highly negative $\delta^{34}S$ values of between −39.7‰ and −12.8‰ that are interpreted to reflect MSR-associated fractionation

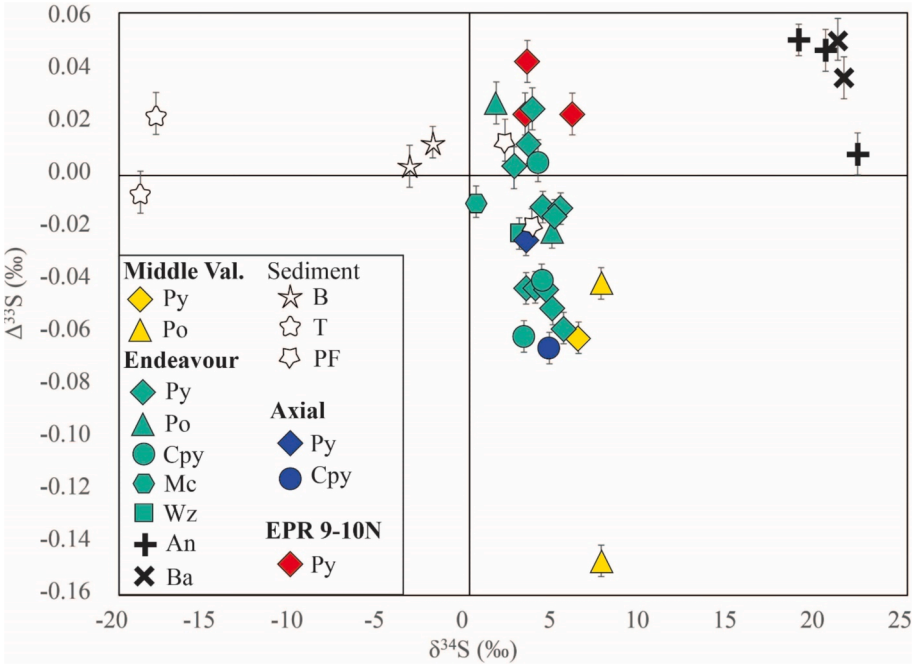

Fig. 6. Results from multiple S isotope analyses displayed by mineralogy, sediment type where 'B' denotes basalt-rich, 'T' denotes turbiditic, and 'PF' denotes plume fallout, and location. Error bars for the y-axis are 1σ, while x-axis 1σ error bars are smaller than the size of the symbols.

Table 2
Results of S isotope analyses of sulfate mineral separates from the Juan de Fuca Ridge.

Sample	Location	Vent area	Mineral	$\delta^{34}S$ (‰)	±1σ (‰)	$\Delta^{33}S$ (‰)	±1σ (‰)
ALV4450-1538	Endeavour	Mothra	An	22.1	0.2	0.008	0.006
ALV4450-1829	Endeavour	Mothra	Ba	21.0	0.2	0.052	0.008
ALV4451-1725	Endeavour	Sasquatch	An	18.8	0.2	0.052	0.008
ALV4522-1748	Axial	International District	An	20.3	0.2	0.048	0.008
D264-R22	Endeavour	MEF	Ba	21.4	0.2	0.037	0.008

An = anhydrite, ba = barite.

Table 3
Results of S isotope analyses of bulk sediments from the Endeavour segment of the Juan de Fuca Ridge as well as visually estimated basaltic glass content.

Sample	Type	Composition	Basaltic Glass (%)	$\delta^{34}S$ (‰)	±1σ (‰)	$\Delta^{33}S$ (‰)	±1σ (‰)
J2-1102–2-PC1	Push core	Plume fallout	< 1	3.6	0.2	−0.019	0.006
J2-1102–4-PC1	Push core	Plume fallout	< 1	2.0	0.2	0.013	0.008
J2-1102–6-PC2	Push core	Turbiditic/pelagic	20	−3.4	0.2	0.004	0.008
J2-1101–9-PC1	Push core	Turbiditic/pelagic	10	−2.1	0.2	0.013	0.006
J2-1102–7-PC1	Push core	Turbiditic/pelagic	2	−17.9	0.2	0.024	0.008
J2-1103–5-PC1	Push core	Turbiditic/pelagic	< 1	−18.8	0.2	−0.006	0.008

(Goodfellow and Blaise, 1988). Similar to these previous studies, the relatively high $\delta^{34}S$ values of the vent sulfide samples compared to the sediment samples indicate that entrainment of microbially reduced sedimentary S into the hydrothermal systems is not a significant process at Middle Valley. This study presents the first $\Delta^{33}S$ values for hydrothermal deposits along the Juan de Fuca Ridge. It was hypothesized that higher $\Delta^{33}S$ values should occur in the sulfide deposits at sedimented Middle Valley relative to sediment-free Axial volcano due to entrainment of reduced microbially-derived sedimentary S into the circulating hydrothermal fluids (e.g., McDermott et al., 2015). Instead, the $\Delta^{33}S$ values from Middle Valley are, on average, more negative than the values for Axial or Endeavour. Therefore, the $\Delta^{33}S$ values agree with the implications from the $\delta^{34}S$ values that the accumulation of turbiditic sediments (documented at Middle Valley, inferred buried at Endeavour) does not appear to be a major influence on the S isotope compositions at these sites.

The $\delta^{34}S$ and $\Delta^{33}S$ values for sulfate minerals from this study (Table 2; Figs. 5, 6) are consistent with most other previously published MOR sulfate mineral S isotope values (e.g., Hughes et al., 2023; Jaeschke et al., 2014; Chiba et al., 1998) and generally indicate a direct seawater sulfate source with minimal to no hydrothermally sourced S or fractionation (Fig. 7; Tostevin et al., 2014; Johnston et al., 2014; Ono et al., 2012, Eickmann et al., 2014; Jaeschke et al., 2014). The two barite samples have both $\delta^{34}S$ and $\Delta^{33}S$ values that closely match that of seawater, whereas the $\delta^{34}S$ and $\Delta^{33}S$ values for the three anhydrite samples show more variability (Fig. 6, 8). This difference may be due to the relative susceptibility of anhydrite to redissolution and reworking versus barite, which, once precipitated, is stable over a wide range of temperatures (Janecky and Seyfried, 1984; Jamieson et al., 2016). However, the current dataset is limited, and more analyses would be

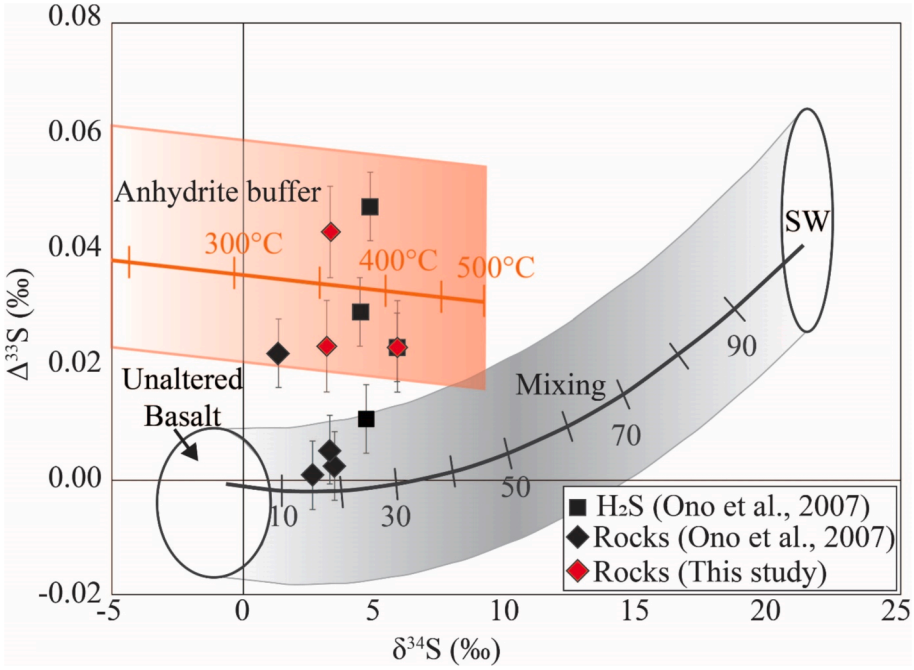

Fig. 7. Isotopic composition of hydrothermal rock and fluid (H_2S) samples from EPR 9-10°N. The orange line represents anhydrite buffering using average seawater S isotope values of 21.3‰ and 0.041‰ for $\delta^{34}S$ and $\Delta^{33}S$, respectively (Johnston et al., 2014; Eickmann et al., 2014; Tostevin et al., 2014; Ono et al., 2012; Aoyama et al., 2014). The surrounding orange box represents the range of buffered compositions considering the variability of modern seawater $\Delta^{33}S$ values (n = 91, using 90% of available data to remove outliers). The curved line represents mixing between reduced S derived from average unaltered basalt (−0.66‰ and −0.001‰ for $\delta^{34}S$ and $\Delta^{33}S$, respectively; Ono et al., 2012; Peters et al., 2010; Peters et al., 2011; n = 6, range again defined by 90% of the data to remove outliers) and reduced seawater sulfate (SW) at various percent seawater influence. The surrounding grey box represents the range of possible values given the uncertainty in the isotopic composition of both endmember reservoirs. Error bars for $\Delta^{33}S$ are 1σ, while $\delta^{34}S$ error bars are smaller than the size of symbols.

needed to validate this trend.

The $\delta^{34}S$ and $\Delta^{33}S$ values of the sediments collected both on– and off-axis along the Endeavour Segment show distinct influences of respective sulfide and basalt glass shard content. The two plume fallout samples (Table 2) have $\delta^{34}S$ and $\Delta^{33}S$ values consistent with those of hydrothermal sulfide mineral separates from this study (Figs. 5, 6). As expected, the basalt-rich samples have slightly negative $\delta^{34}S$ values with positive $\Delta^{33}S$ values, consistent with a mix of S sourced from relatively unaltered basalt and biogenically influenced sediment (Fig. 8). The two turbidite-dominated samples have $\delta^{34}S$ values that are comparable to what is expected for sedimentary sulfide produced by MSR (e.g., Shanks et al., 1995, Canfield, 2001; Figs. 6, 8). However, the $\Delta^{33}S$ values of these two samples differ. The sample composed almost exclusively of turbiditic material has a positive $\Delta^{33}S$ value that is consistent with a biogenic sedimentary source. The other sample is dominated by turbiditic sediment but also contains ~2% basalt material. It has a negative $\Delta^{33}S$ value and plots outside of the compositional field expected for a biogenic sedimentary source on a mixing line with altered basalt (Fig. 8; McDermott et al.,2015; Peters et al., 2010; Peters et al., 2011). These results indicate that microbially-derived reduced S content in the turbiditic sediments at Endeavour is likely so low that even a minor amount of basalt can significantly affect the S isotope composition, particularly with respect to the highly sensitive $\Delta^{33}S$ values. While this is a plausible explanation for the sediment S isotope signatures from Endeavour, the limited data set presented in this study necessitates additional analyses, including S concentration, in order to validate this possibility.

5.3. Origin of negative $\Delta^{33}S$ values

Two-component mixing between unaltered igneous S and seawater sulfate can only produce products with positive or near zero $\Delta^{33}S$ values (Fig. 7). Additional equilibration through isotopic exchange with anhydrite will only drive these values further in the positive direction, as is the case at EPR 9-10°N (Fig. 7). While some of the sulfide samples from Endeavour have S isotope signatures consistent with the two-component mixing and anhydrite buffering, most of the Juan de Fuca Ridge samples have $\Delta^{33}S$ values that are too low for the dominant process to be simple mixing and anhydrite buffering. Although samples with more negative $\Delta^{33}S$, accompanied by slightly higher $\delta^{34}S$ values, are still likely affected by two-component mixing and anhydrite buffering, they additionally require a mixing model with endmember compositions that differ from the standard igneous values for oceanic crust and typical seawater values, such that could be achieved through microbial alteration of oceanic crust (Fig. 8).

5.3.1. Microbially-altered oceanic crust

Along the Juan de Fuca Ridge, open-system MSR in the subsurface produced significantly negative S isotope values in the basaltic crust (as low as −29‰ and −0.057‰ for both $\delta^{34}S$ and $\Delta^{33}S$, respectively; Ono et al., 2012). Low-temperature microbial alteration of host rocks and progressive fluid-rock interaction thereafter can produce reduced S products with both negative $\delta^{34}S$ and $\Delta^{33}S$ values, resulting in deviation from two-component mixing models (Fig. 8; c.f., Ono et al., 2012). These results indicate that hydrothermal fluids flowing through basaltic crust that has been previously microbially altered can acquire a reduced crustal S component that has already undergone microbially mediated isotopic fractionation resulting in more negative $\delta^{34}S$ and $\Delta^{33}S$ values. The isotopic fractionations associated with this process would be most pronounced at hydrothermal sites hosted on older and therefore potentially more microbially-altered crust. Age constraints on hydrothermal sulfide deposition along the Juan de Fuca Ridge indicate crustal ages (i.e., inferred age of the crust underlying sulfide deposits) of at least 3,000 years at Endeavour and at least 16,000 years at Middle Valley (Jamieson et al., 2013; Scholten et al., 2000; Davis and Lister, 1977), and are consistent with more negative $\Delta^{33}S$ values associated with hydrothermal circulation through older crust (Fig. 8). No age constraints

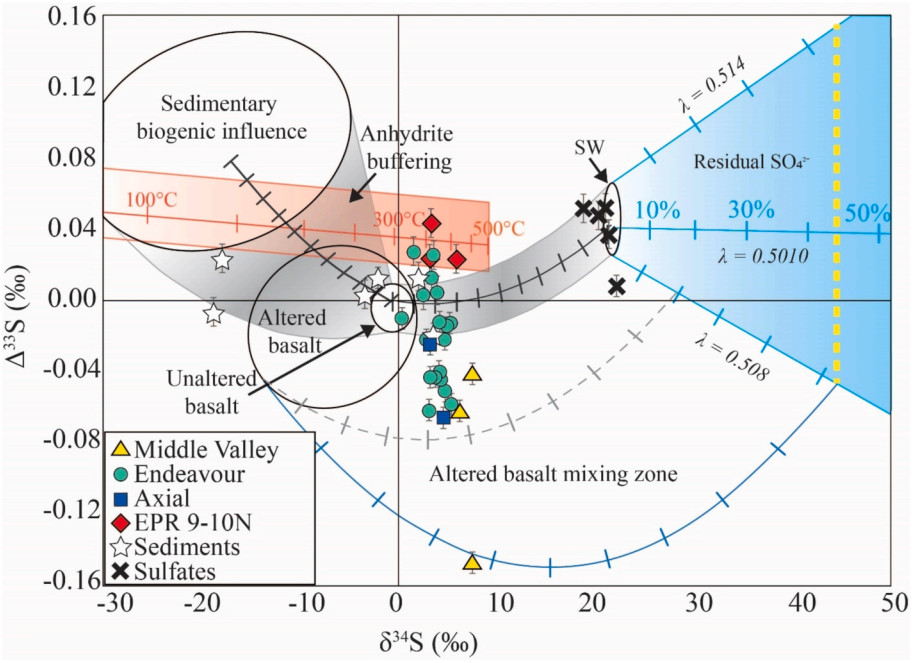

Fig. 8. Multiple S isotope data from this study presented on a mixing and fractionation model where curved lines represent mixing between average values of various S reservoirs at 10% intervals with grey representing general main mixing range. Ovals represent 90% of previously reported data for endmember S reservoirs (Sedimentary biogenic S: n = 19; Juan de Fuca Ridge microbially altered basalt: n = 52; unaltered basalt; n = 6; Seawater [SW]: n = 91). Straight lines represent fractionation via anhydrite buffering at different temperatures (orange) and residual SO_4^{2-} (blue) at different percent residual SO_4^{2-}. The different residual SO_4^{2-} lines denote the range in fractionation factors at different λ^{33} values measured for sulfate reduction in modern microbial systems (Johnston, 2011; Tostevin et al., 2014). Data retrieved from: Peters et al., 2010; Peters et al., 2011; McDermott et al., 2015; Ono et al., 2007; Ono et al., 2012; Tostevin et al., 2014; Johnston et al., 2014; Eickmann et al., 2014; Aoyama et al., 2014. The blue curved line represents the extent of known potential mixing between Juan de Fuca Ridge altered basalt (Ono et al., 2012) and barite with a residual SO_4^{2-} component from sub-seafloor Middle Valley (Adshead, 1996; $\delta^{34}S$ = 44.5‰, represented by a yellow dashed line) projected onto the extent of MSR at λ^{33} = 0.508. The grey dashed curved line represents an example mixing line between the extent of altered Juan de Fuca Ridge basalt and a ~20% residual SO_4^{2-} component. Error bars for $\Delta^{33}S$ are 1σ, while $\delta^{34}S$ error bars are smaller than the size of symbols.

are available for hydrothermal deposits at Axial volcano, but volcanic eruptions as recent as 2015 have been documented (Wilcock et al., 2016). However, the relatively more negative $\Delta^{33}S$ values recorded from the samples collected from the International District within the volcano caldera suggest that the basaltic substrate here has also undergone a significant degree of microbial alteration. Interestingly, Butterfield et al. (2004) reported the presence of thermophilic sulfate-reducing microbes in diffuse fluids at Axial volcano. These fluids were venting at temperatures lower than the optimum growth conditions for these specific microbes (>80 °C), potentially indicating a higher temperature origin in the subsurface. Similarly, drilled 3.5 million-year-old basaltic crust on the flank of Juan de Fuca Ridge has shown biogeochemical evidence of significant MSR activity, including highly negative $\delta^{34}S$ values (Lever et al., 2013). Fluid sampling from CORK (Circulation Obviation Retrofit Kit) borehole observatories located on 1.2 and 3.5 million-year-old crust, also on the ridge flank of the Juan de Fuca Ridge, again resulted in the identification of prevalent sulfate reducing bacteria in warm (~65 °C) anoxic basement fluids (Jungbluth et al., 2017). The presence of thermophilic sulfate reducers in basement fluids is consistent with microbially mediated sub-seafloor sulfate reduction and associated microbial alteration at depth within the high temperature sub-seafloor hydrothermal system. However, MSR is not necessarily a hydrothermal process and is happening everywhere the necessary conditions (such as available electron acceptors and donors) are met at temperatures able to support life (i.e., between ambient bottom seawater: ~2 °C and potentially up to the maximum temperature hyperthermophiles can survive: ~120 °C; c.f. Ono et al., 2012; Takai et al., 2008). Notably, this temperature range is lower than the fluid temperature which can mobilize sulfide minerals (>150 °C; Giggenbach, 1974) and thus these processes are not considered to be occurring in tandem.

Within the Endeavour vent field, the S isotope compositions of samples from Zephyr Mound have more negative $\Delta^{33}S$ values than samples from MEF, High Rise, Salty Dawg, and Sasquatch. Zephyr Mound is the largest known massive sulfide occurrence at Endeavour and is unique within the Endeavour field because it is situated on older crust (at least 3,000 years old) outside of the main rift valley floor (Fig. 2; Jamieson et al., 2013; Jamieson et al., 2014). Due to its much larger size than the other vent deposits at Endeavour, Zephyr Mound likely formed over a prolonged period, leading to a higher degree of microbial alteration in the subsurface, and a more negative $\Delta^{33}S$ isotopic signature.

In contrast to the older, and likely more microbially altered crust at Endeavour and Middle Valley, the EPR 9-10°N site is hosted on a more volcanically-active, fast-spreading segment that has experienced several eruptions in recent decades (Fornari et al., 2012). Here, the relatively fresh crust has likely not undergone the same degree of microbial alteration and the hydrothermal fluids would not yet have acquired a fractionated reduced S signature that characterizes hydrothermal systems hosted within older crust (i.e., relatively higher $\delta^{34}S$ values coupled with more negative $\Delta^{33}S$ values). The assessment of crustal age at Axial volcano is more complex, as it has experienced several recent eruptions (e.g. 1998, 2011, 2015; Caress et al., 2012; Embley et al., 1999; Wilcock et al., 2016). However, the volcano is also located on the intermediate-rate spreading Juan de Fuca Ridge, and therefore on relatively older crust than EPR, resulting in the potential for the sub-seafloor hydrothermal fluids at Axial to flow through crustal rocks of a wide range of ages and degrees of microbial alteration.

Sulfide minerals from hydrothermal sites at slow spreading ridges, such as Logatchev, TAG, and Rainbow on the Mid-Atlantic Ridge (average sulfide deposit $\delta^{34}S$ values of 6.5‰, 6.7‰, and 7.6‰, respectively; Bogdanov et al., 1997; Bogdanov et al., 2002; Dubinina et al., 2020; Zeng et al., 2017; Lein et al., 2001; Herzig et al., 1998; Gemmell

and Sharpe, 1998; Friedman, 1998; Knott et al., 1998; Glynn et al., 2006; Stuart et al., 1994a; Chiba et al., 1998), have $\delta^{34}S$ values that are higher than typical EPR values, similar to the Middle Valley samples analyzed here. Uranium-series disequilibrium dating of the hydrothermal deposits at these Mid-Atlantic Ridge hosted sites indicate that, again like Middle Valley, the deposits are hosted on crust that is well over 15,000 years old (Kuznetsov et al., 2006; Lalou et al., 1995). The higher $\delta^{34}S$ values at these sites also contrasts the lower $\delta^{34}S$ values at relatively younger hydrothermal sites such as Lucky Strike (average sulfide-rich rocks $\delta^{34}S$ value = 2.3‰; Ono et al., 2007; Sánchez-Mora, et al., 2022; Rouxel et al., 2004). Currently, only $\delta^{34}S$ values are reported for these sites, and measurements of $\Delta^{33}S$ would be required to further investigate whether the $\Delta^{33}S$ versus $\delta^{34}S$ trend identified in the Juan de Fuca Ridge and EPR samples, and the relationship of this trend to ages of hydrothermal systems and degree of microbial alteration of the underlying crust, applies to other tectonic settings.

5.3.2. Residual seawater sulfate

Hydrothermal circulation through older crust results in the enrichment of ^{34}S in hydrothermal minerals due to the mixing of S sourced from increasingly microbially altered basalt. The precipitation of H_2S produced during MSR as biogenic sulfide preferentially removes light S isotopes from circulating hydrothermal fluid and generates isotopically heavy residual sulfate with a $\delta^{34}S$ value greater than the starting seawater sulfate value that is subsequently thermochemically reduced and mixed with altered basalt-derived S. The preferential removal of isotopically light sulfate by MSR in the sub-seafloor thus produces a progressively isotopically heavy residual sulfate pool, with the magnitude of the higher $\delta^{34}S$ values dependent on the relative degree of reduction of the original seawater sulfate pool (Fig. 8; e.g., Aoyama et al., 2014). At Middle Valley, isotopically heavy barite samples, with sulfate $\delta^{34}S$ values as high as 44.5‰, were collected from sediment cores 6 m below the seafloor (Adshead, 1996). The subseafloor barite therefore provides a record of the isotopic composition of residual sulfate that remains following MSR within the sediment at Middle Valley.

The λ-value for MSR in marine settings is variable, ranging from 0.508 to 0.514 (Johnston, 2011; Tostevin et al., 2014), and resulting in a residual sulfate field defined by $\delta^{34}S$ values that are greater than seawater, but $\Delta^{33}S$ values that could be either higher or lower than seawater values (Fig. 8). Mixing of microbially altered or unaltered reduced igneous S with residual sulfate will generate increasingly negative $\Delta^{33}S$ values. The magnitude of the possible negative $\Delta^{33}S$ values would be dependent on both the degree of reduction of the original seawater sulfate pool (denoted by isotopically heavy Middle Valley sulfate; Fig. 8) and the λ-value of the fractionation process (with lower λ-values resulting in more negative $\Delta^{33}S$ values). The majority of Juan de Fuca Ridge sulfide samples have S isotope signatures consistent with mixing of S derived from microbially altered basalt mixed with a ~20% microbially fractionated and reduced residual seawater S source (grey dashed line Fig. 8). However, the influence of a residual sulfate pool would likely be greatest in sedimented environments, which is consistent with the Middle Valley samples in this study having, on average, isotopic compositions with the most negative $\Delta^{33}S$ values. An outlier sample from Middle Valley that has a highly negative $\Delta^{33}S$ value (−0.147‰) falls along a mixing line defined by the altered basalt mixing zone and a value for partially reduced seawater sulfate defined by the maximum $\delta^{34}S$ values recorded for sedimentary barite at Middle Valley (Adshead, 1996). Hence, this sample may have been influenced by the greater potential of highly fractionated residual SO_4^{2-} at the sedimented Middle Valley vs. the other sites. Overall, the linear array defined by the combined $\delta^{34}S$ and $\Delta^{33}S$ compositions of the sulfide-rich rock samples from the Juan de Fuca Ridge indicates a S source controlled by relatively uniform mixing between two S reservoirs (i.e., altered basalt and residual SO_4^{2-}) that have both experienced varying degrees of a microbial modification to their respective isotopic compositions.

5.4. Endmember evolution and the deep biosphere

Hydrothermal S cycling at MORs can be influenced by a wide range of geological and biological factors (e.g., Chiba et al., 1998; Shanks et al., 1995; Shanks, 2001; Sánchez-Mora et al., 2022; Ono et al., 2007; McDermott et al., 2015; Hannington et al., 2005; Peters et al., 2010; Peters et al., 2011; Eickmann et al., 2014). While individual sites may be affected by numerous mixing and isotopic fractionation processes, our model (Fig. 8) allows for the recognition and differentiation of several different processes and geological settings, the results of which are summarized in Fig. 9. These results indicate that crustal age, its associated microbial alteration, and spreading rate all play a key role in S cycling at MOR hydrothermal systems, with sites situated on older, more altered, slower-spreading seafloor crust having more positive $\delta^{34}S$ values coupled with generally more negative $\Delta^{33}S$ values for sulfide minerals. While our results and model may be generally applicable to MORs across the broader seafloor, they may also provide insight into S cycling throughout the global ocean crust as a whole.

Rouxel et al. (2008) recorded similar negative multiple S isotope values (i.e., average $\delta^{34}S$ and $\Delta^{33}S$ values of −17.5‰ and −0.061‰, respectively) for altered basalt from the western Pacific to those measured from altered Juan de Fuca Ridge basalt by Ono et al. (2012) presented in our model (Fig. 9). The western Pacific altered basalt was collected from Jurassic-aged oceanic crust underlying the Magellan Seamounts, located on the abyssal plain proximal to the Mariana Trench and is representative of some of the oldest modern seafloor (Rouxel et al., 2008). These similar basaltic S isotopic compositions between these two locations suggests similar microbial processes and associated S isotope fractionations for basaltic oceanic crust over a broad range of ages. However, while our model for S isotope compositions based on age and related subseafloor microbial alteration may be broadly applicable at the system scale, variations, especially at the sample or single vent scale are likely to occur. The pathways for hydrothermal recharge into the basement rock remain unconstrained. Thus, hydrothermal S flux and related microbially sourced S variations could also potentially be a function of highly variable circulation pathways between different hydrothermal systems. Variable local ingress of seawater at vent sites may facilitate both MSR and TSR within hydrothermal mineral deposits, contributing to the isotopically heavy S signatures of both sulfide and sulfate minerals documented at TAG, Middle Valley, and the Piccard field on the Mid-Cayman Rise (Fig. 9; e.g., Chiba et al., 1998; Duckworth et al., 1994; McDermott et al., 2020). Similarly, circulation pathways and hydrothermally permeability will be modified by igneous intrusions, faulting, and progressive hydrothermal alteration (e.g., Davis et al., 1992; Fontaine et al., 2001). Such variations may be more pronounced at arc-related settings where hydrothermal alteration from low-pH fluids and the potential addition of volcanic SO_2 as a primary S source provide additional complexity (e.g., LaFlamme et al., 2018). On slow- and ultraslow-spreading ridges, similar complexity affecting ultramafic-hosted systems due to serpentinization reactions associated with sub-seafloor alteration must also be considered (c.f., Ono et al., 2012; Schwarzenbach et al., 2018).

The deep marine basaltic subsurface biosphere is the largest biosphere on Earth, but our understanding of this biosphere, including its global significance and sustaining features, remains poorly understood (Orcutt et al., 2013; Gittins et al., 2022; Cario et al., 2019, Klein et al., 2015; Biddle et al., 2012). Our study adds to the growing body of literature documenting the impact of the deep biosphere on oceanic biogeochemical cycling, as well as fluid cycling at hydrothermal systems (e.g., Goordial et al., 2021; Orcutt et al., 2011; Orcutt et al., 2013; Cario et al., 2019). Our results indicate that active hydrothermal systems may be of under-recognized importance for linking such biosphere-geosphere interactions in the subseafloor to the global ocean as a whole.

While our study investigates the potential of subseafloor microbial alteration affecting seafloor hydrothermal S cycling, it also highlights the utility and potential of multiple S isotopes to delineate and identify

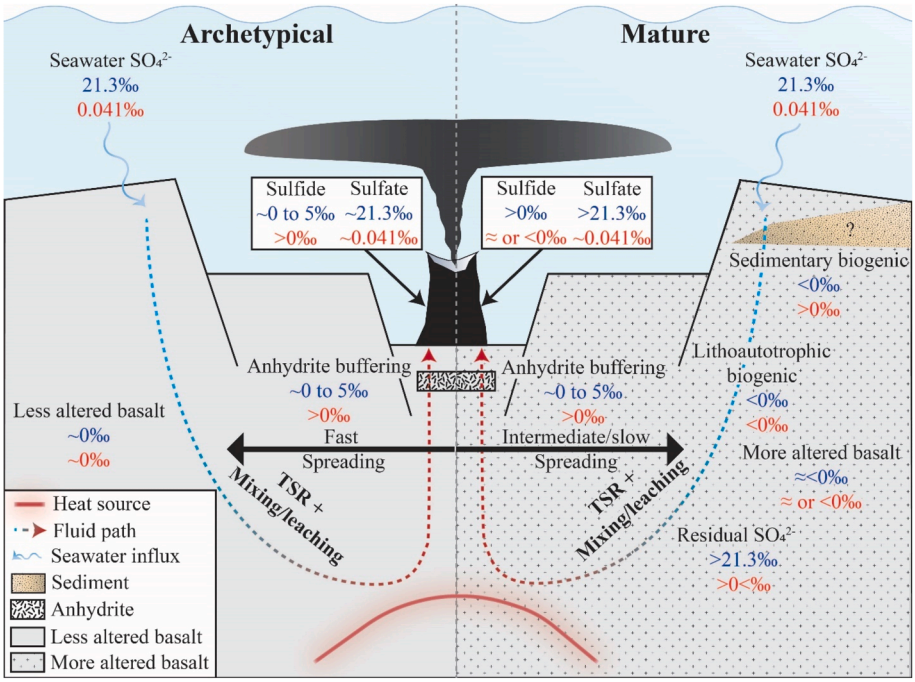

Fig. 9. Schematic of mid-ocean ridge hydrothermal circulation showing general isotopic compositions of S reservoirs, fractionation processes, and resultant hydrothermally precipitated sulfate and sulfide S isotope signatures at both mature and archetypical hydrothermal systems discussed in text (Alt et al., 2003; Chiba et al., 1998; Tostevin et al., 2014; Eickmann et al., 2014; Johnston et al., 2014; Ono et al., 2007; Ono et al., 2012; Peters et al., 2010; Peters et al., 2011; Aoyama et al., 2014; McDermott et al., 2015; Adshead, 1996). Blue text represents typical $\delta^{34}S$ values, while red text denotes $\Delta^{33}S$ values for each labelled S reservoir and process. "Sediment" in this context refers to turbiditic/pelagic-sourced sediment. Thermochemical sulfate reduction is denoted as "TSR." The anhydrite buffering range is based on maximum vent temperatures measured at sites from this study (i.e., ~300 – 400 °C; Delaney et al., 1992; Kelley et al., 2001; Holden, 2015; Ames et al., 1993; Kelley et al., 2014; Von Damm, 2000). This figure is a schematic only, and not to scale. The location of hydrothermal recharge is only illustrative, as the location of hydrothermal recharge is still not fully constrained.

otherwise-unrecognized complexity associated with hydrothermal processes in more complicated altered systems overall. Here we show that endmember S reservoirs can have varying isotopic compositions and these compositions can evolve, causing isotope variations related to age and geologic setting. Thus, initial basalt S reservoir isotopic compositions have significant variability in average S isotope compositions between more altered, mature and less altered MOR spreading centers (Rouxel et al., 2008, Ono et al., 2012; Schwarzenbach et al., 2018). Such endmember evolutionary processes may be applicable to the broader seafloor, including to both biogenically and non-biogenically altered systems across geologic time. For example, Aoyama et al. (2018) documented altered Archean crustal material influencing modern hydrothermal S cycling in Mariana forearc serpentinite mud volcanoes. Similarly, Alt et al. (2003) documented entrainment of residual sulfate produced by MSR during axial hydrothermal circulation from S isotopic analyses of the Macquarie Island ophiolite. Thus, the processes outlined in our study may be applicable to not only basalt-hosted systems and relatively young ophiolites like Macquarie Island, but to hydrothermal S cycling in the modern and ancient rock record as a whole.

6. Conclusions

New multiple S isotope data from sulfide and sulfate minerals sampled at three sites along the Juan de Fuca Ridge (Middle Valley, Axial Volcano, Endeavour), in comparison with samples from EPR 9-10°N, have resulted in a refined understanding of hydrothermal processes at these sites. Our results additionally further confirm previous reports of reduced S in hydrothermal sulfide deposits from EPR 9-10°N that is derived from two-component mixing between unaltered basalt and seawater and subsequent anhydrite buffering. These new data further demonstrate the potential for multiple S isotopes ($\delta^{33}S$ and $\Delta^{33}S$ in addition to $\delta^{34}S$) to identify geological and microbial processes associated with S cycling in submarine hydrothermal systems that are otherwise not resolvable with the more traditionally reported linear $\delta^{34}S$ values. A summary of the key findings based on our work is:

1. Ranges in $\delta^{34}S$ values for seafloor hydrothermal sulfide deposits that were previously interpreted to result from either natural variability in isotopic compositions or varying degrees of two component mixing between igneous S and seawater sulfate may instead be due to microbial isotopic fractionation and subsequent entrainment of reduced S in the igneous basement. The relative degree of subsurface microbial fractionation is linked to the progressive microbial alteration of crust over time.
2. Microbial isotopic fractionation of seawater sulfate can also change the isotopic composition of seawater sulfate in the downwelling recharge fluid.
3. Sulfur leached from sediments is not a significant component of the S in seafloor hydrothermal deposits at MORs.
4. Hydrothermal fluid cycling through microbially altered oceanic crust may provide critical links between the deep marine subsurface basaltic biosphere and the global ocean.
5. Isotopic endmember compositions of S reservoirs associated with submarine hydrothermal circulation can be variable and evolve over time.

CRediT authorship contribution statement

Sarah N. Moriarty: Conceptualization, Methodology, Validation, Formal analysis, Investigation, Resources, Data Curation, Writing – original draft, Writing – review & editing, and Visualization. **Emma Bertran:** Writing – review & editing, Validation, Investigation. **James**

W. Dottin: Writing – review & editing, Validation, Investigation. **James Farquhar:** Writing – review & editing, Validation, Methodology, Investigation. **David T. Johnston:** Writing – review & editing, Validation, Methodology, Investigation. **Stephen J. Piercey:** Writing – review & editing, Resources. **Dennis Sánchez-Mora:** Writing – review & editing, Resources. **Michael G. Babechuk:** Writing – review & editing. **Jason B. Sylvan:** Writing – review & editing, Resources, Funding acquisition. **John W. Jamieson:** Writing – review & editing, Visualization, Validation, Supervision, Resources, Project administration, Methodology, Investigation, Funding acquisition, Formal analysis, Data curation, Conceptualization.

Data availability

Data are available through Zenodo at https://doi.org/10.5281/zenodo.12823830.

Declaration of competing interest

The authors declare that they have no known competing financial interests or personal relationships that could have appeared to influence the work reported in this paper.

Acknowledgements

The authors would like to acknowledge and thank the scientists and crew aboard the *R/V Atlantis* cruises AT15-36 (2008), AT15-47 (2009), AT42-21 (2019-2020), the *R/V Western Flyer* (MBARI, 2011), the *CCGS Tully* (Fisheries and Oceans Canada, 2016), and *R/V Kilo Moana* KM1812 (2018) research cruises for their preliminary sampling data collection. J. W.J. acknowledges financial support from the Canada Research Chairs program (CRC-2020-001165) and a Natural Sciences and Engineering Research Council of Canada (NSERC) Discovery Grant (RGPIN-2017-05548). S.N.M. acknowledges funding support from the NSERC Collaborative Research and Training Experience (CREATE) project in Marine Geodynamics and Georesources program (iMAGE; 545104-2020). J.B.S acknowledges funding from the National Science Foundation (OCE 1756339). The authors would like to thank Jeff Alt and one anonymous reviewer for their helpful comments, as well as Esther Schwarzenbach for comments and editorial handling.

References

Achberger, A.M., Jones, R., Jamieson, J., Holmes, II, C.P., Schubotz, F., Meyer, N.R., Dekas, A.E., Moriarty, S., Reeves, E.P., Manthey, A., Brüenjes, J., Daniel J. Fornari, D.J., Tivey, M.K., Toner, B.M, Sylvan, J.S., 2024. Inactive Hydrothermal Vent Deposits are Important Sites for Primary Productivity in the Deep Ocean. Nat. Microbiol. 9, 657–668.

Adshead, J.D., 1996. Stable isotopes, ^{14}C dating, and geochemical characteristics of carbonate nodules and sediment from an active vent field, northern Juan de Fuca Ridge, Northeast Pacific. Chem. Geol. 129, 133–152.

Alt, J.C., 1995a. Subseafloor Processes in Mid-Ocean Ridge Hydrothermal Systems. Geophys. Monogr. 91, 85–114.

Alt, J.C., 1995b. Sulfur isotopic profile through the oceanic crust: Sulfur mobility and seawater-crustal sulfur exchange during hydrothermal alteration. Geology 23, 585–588.

Alt, J.C., Anderson, T.F., Bonnell, L., 1989. The geochemistry of sulfur in a 1.3 km section of hydrothermally altered oceanic crust, DSDP Hole 504B. Geochim. Cosmochim. Acta 53, 1011–1023.

Alt, J.C., Davidson, G.J., Teagle, D.A.H., Karson, J.A., 2003. Isotopic composition of gypsum in the Macquarie Island ophiolite: Implications for the sulfur cycle and the subsurface biosphere in oceanic crust. Geology 31, 549–552.

Ames, D.E., Franklin, J.M., Hannington, M.D., 1993. Mineralogy and geochemistry of active and inactive chimneys and massive sulfide, Middle Valley, northern Juan de Fuca Ridge; an evolving hydrothermal system*. Canad. Mineral. 31, 997–1024.

Aoyama, S., Nishizawa, M., Junichi, M., Shibuya, T., Ueno, Y., Takai, K., 2018. Recycled Archean sulfur in the mantle wedge of the Mariana Forearc and microbial sulfate reduction within an extremely alkaline serpentinite seamount. Earth Planet. Sci. Lett. 491, 109–120.

Aoyama, S., Nishizawa, M., Takai, K., Uenoa, Y., 2014. Microbial sulfate reduction within the Iheya North sub-seafloor hydrothermal system constrained by quadruple sulfur isotopes. Earth Planet. Sci. Lett. 398, 113–126.

Aquino, K.A., Früh-Green, G.L., Rickli, J., Bernasconi, S.M., Lang, S.Q., Lilley, M.D., Butterfield, D.A., 2022. Multi-stage evolution of the Lost City hydrothermal vent fluids. Geochim. Cosmochim. Acta 332, 239–262.

Bach, W., Edwards, K.J., 2003. Iron and sulfide oxidation within the basaltic ocean crust: implications for chemolithoautotrophic microbial biomass production. Geochim. Cosmochim. Acta 67, 3871–3887.

Beaudoin, G., Taylor, B.E., Rumble III, D., Thiemens, M., 1994. Variations in the sulfur isotope composition of troilite from the Cañon Diablo iron meteorite. Geochim. Cosmochim. Acta 58, 4253–4255.

Biddle, J.F., Sylvan, J.B., Brazelton, W.J., Tully, B.J., Edwards, K.J., Moyer, C.L., Heidelberg, J.F., Nelson, W.C., 2012. Prospects for the study of evolution in the deep biosphere. Front. Microbiol. 2.

Bogdanov, Y.A., Bortnikov, N.S., Sagalevich, A.M., Gurvich, E.G., Vikentev, I.V., 1997. New type of mineral-forming systems: Black smokers of the hydrothermal field at 14° 45'N MAR. Geologiya Rudnykh (Geology of Ore Deposits) 39, 68–90.

Bogdanov, Y.A., Bortnikov, N.S., Vikentev, I.V., Lein, A.Y., Gurvich, E.G., Sagalevich, A. M., Anatoly, M., Simonov, V.A., Ikorsky, S.V., Stavrova, O.O., Apollonov, V.N., 2002. Mineralogical-geochemical peculiarities of hydrothermal sulfide ores and fluids in the rainbow field associated with Serpentinites, Mid-Atlantic Ridge (36°14'). Geology of Ore Deposits 44, 444–473.

Butterfield, D.A., Roe, K.K., Lilley, M.D., Huber, J.A., Baross, J.A., Embley, R.W., Massoth, G.J., 2004. Mixing, Reaction and Microbial Activity in the Sub-seafloor Revealed by Temporal and Spatial Variation in Diffuse Flow Vents at Axial Volcano: The Sub-seafloor Biosphere at Mid-Ocean Ridges. Geophys. Monogr. 144, 267–285.

Canfield, D.E., 2001. Biogeochemistry of sulfur isotopes. Rev. Mineral. Geochem. 43, 607–636.

Canfield, D.E., Raiswell, R., Westrich, J.T., Reaves, C.M., Berner, R.A., 1986. The use of chromium reduction in the analysis of reduced inorganic sulfur in sediments and shales. Chem. Geol. 54, 149–155.

Caress, D.W., Clague, D.A., Paduan, J.B., Martin, J.F., Dreyer, B.M., Chadwick Jr, W.W., Denny, A., Kelley, D.S., D.s., 2012. Repeat bathymetric surveys at 1-metre resolution of lava flows erupted at Axial Seamount in April 2011. Nat. Geosci. 5, 483–488.

Cario, A., Oliver, G.C., Rogers, K.L., 2019. Exploring the Deep Marine Biosphere: Challenges, Innovations, and Opportunities. Front. Earth Sci. 7.

Chadwick, J., Perfit, M., Ridley, I., Jonasson, I., Kamenov, G., Chadwick, W., Embley, R., le Roux, P., Smith, M., 2005. Magmatic effects of the Cobb hot spot on the Juan de Fuca Ridge. J. Geophys. Res. Solid Earth 110.

Chiba, H., Uchiyama, N., Teagle, D.A.H., 1998. Stable isotope study of anhydrite and sulfide minerals at the TAG hydrothermal mound, Mid-Atlantic Ridge, 26°N. In: Proceedings of the Ocean Drilling Program, Scientific Results 158, 85–90.

Clague, D., Caress, D., 2015. Processed Near-bottom Multibeam Sonar Data from the Juan de Fuca Spreading Center - Endeavour Segment acquired during the Zephyr expedition ZPR1108 (2011). In: Interdisciplinary Earth Data Alliance (IEDA).

Clague, D.A., Paduan, J.B., Dreyer, B.M., Chadwick II, W.W., Rubin, K.R., Perfit, M.R., Fundis, A.T, 2018. Chemical Variations in the 1998, 2011, and 2015 Lava Flows From Axial Seamount, Juan de Fuca Ridge: Cooling During Ascent, Lateral Transport, and Flow. Geochem. Geophys. Geosyst. 19, 2915–2933.

Coplen, T.B., Krouse, H.R., 1998. Sulphur isotope data consistency improved. Nature 392, 32.

Cousens, B.L., Blenkinsop, J., Franklin, J.M., 2002. Lead isotope systematics of sulfide minerals in the Middle Valley hydrothermal system, northern Juan de Fuca Ridge. Geochem. Geophys. Geosyst. 3, 1–16.

Cowen, J.P., Giovannoni, S.J., Kenig, F., Johnson, H.P., Butterfield, D.A., Rappe, M.S., Hutnak, M., Lam, P., 2003. Fluids from aging ocean crust that support microbial life. Science 299, 120–123.

Crowe, D.E., Valley, J.W., 1992. Laser microprobe study of sulfur isotope variation in a sea-floor hydrothermal spire, Axial Seamount, Juan de Fuca Ridge, eastern Pacific. Chem. Geol. 101, 63–70.

Cruse, A.M., Seewald, J.S., Saccocia, P.J., Zierenberg, R., 2008. Hydrothermal Fluid Composition at Middle Valley, Northern Juan de Fuca Ridge: Temporal and Spatial Variability. Geophys. Monogr. 178.

Davis, E.E., Fisher, A.T., 1994. On the nature and consequences of hydrothermal circulation in the Middle Valley sedimented rift: inferences from geophysical and geochemical observations, Leg 139. In: Proceedings of the Ocean Drilling Program, Scientific Results 139, 695–717.

Davis, E.E., Goodfellow, W.D., Bornhold, B.D., Adshead, J., Blaise, B., Villinger, H., Le Cheminant, G., 1987. Massive sulphides in a sedimented rift valley, Northern Juan de Fuca Ridge. Earth Planet. Sci. Lett. 82, 49–61.

Davis, E.E., Lister, C.R.B., 1977. Tectonic structures on the Juan de Fuca Ridge. Geol. Soc. Am. Bull. 88, 346–363.

Davis, E.E., Mottl, M.J., Fisher, A.T., Shipboard Scientific Party, 1992. Introduction. In: Proceedings of the Ocean Drilling Program, Initial Reports 139, 5–7.

Davis, E.E., Villinger, H., 1992. Tectonic and thermal structure of the Middle Valley sedimented rift, Northern Juan de Fuca Ridge. In: Proceedings of the Ocean Drilling Program, Initial Reports 139, 9–41.

Delaney, J.R., Robigou, V., McDuff, R.E., Tivey, M.K., 1992. Geology of a vigorous hydrothermal system on the Endeavour Segment, Juan de Fuca Ridge. J. Geophys. Res. Solid Earth 97, 19663–19682.

Ding, T., Valkiers, S., Kipphardt, H., De Bievre, P., Taylor, P.D.P., Gonfiantini, R., Krouse, R., 2001. Calibrated sulfur isotope abundance ratios of three IAEA sulfur isotope reference materials and V-CDT with a reassessment of the atomic weight of sulfur. Geochim. Cosmochim. Acta 65, 2433–2437.

Divins, D.L., 2003. Total Sediment Thickness of the World's Oceans & Marginal Seas. NOAA National Geophysical Data Center, Boulder CO.

Dubinina, E.O., Bortnikov, N.S., Stavrova, O.O., Kossova, S.A., 2020. Sulfur Isotope Fractionation During Sulfide Generation in the Hydrothermal Submarine Systems:

The Case of Logatchev, Krasnov, and Rainbow Hydrothermal Fields, Mid-Atlantic Ridge. Geology of Ore Deposits 62, 351–371.
Duckworth, R.C., Fallick, A.E., Rickard, D., 1994. Mineralogy and sulfur isotopic composition of the Middle Valley massive sulfide deposit, northern Juan de Fuca Ridge. In: Proceedings of the Ocean Drilling Program, Scientific Results 139, 373–385.
Edwards, K.J., Bach, W., Rogers, D.R., 2003. Geomicrobiology of the Ocean Crust: A Role for Chemoautotrophic Fe-Bacteria. Biol. Bull. 204, 180–185.
Eickmann, B., Thorseth, I.H., Peters, M., Strauss, H., Brocker, M., Pedersen, R.B., 2014. Barite in hydrothermal environments as a recorder of sub-seafloor processes: a multiple-isotope study from the Loki's Castle vent field. Geobiology 12, 308–321.
Elderfield, H., Wheat, C.G., Mottl, M.J., Monnin, C., Spiro, B., 1999. Fluid and geochemical transport through oceanic crust: a transect across the eastern flank of the Juan de Fuca Ridge. Earth Planet. Sci. Lett. 172, 151–165.
Eldridge, D.L., Guo, W., Farquhar, J., 2016. Theoretical estimates of equilibrium sulfur isotope effects in aqueous sulfur systems: Highlighting the role of isomers in the sulfite and sulfoxylate systems. Geochim. Cosmochim. Acta 195, 171–200.
Embley, R.W., Chadwick Jr, W.W., Clague, D., Stakes, D., 1999. 1998 eruption of axial volcano: Multibeam anomalies and sea-floor observations. Geophys. Res. Lett. 26, 3425–3428.
Embley, R.W., Murphy, K.M., Fox, C.G., 1990. High-resolution studies of the summit of Axial volcano. J. Geophys. Res. 95, 12785–12812.
Farquhar, J., Bao, H.M., Thiemens, M., 2000. Atmospheric influence of Earth's earliest sulfur cycle. Science 289, 756–758.
Farquhar, J., Johnston, D.T., Wing, B.A., 2007. Implications of conservation of mass effects on mass-dependent isotope fractionations: Influence of network structure on sulfur isotope phase space of dissimilatory sulfate reduction. Geochim. Cosmochim. Acta 71, 5862–5875.
Farquhar, J., Johnston, D.T., Wing, B.A., Habicht, K.S., Canfield, D.E., Airieau, S., Thiemens, M.H., 2003. Multiple sulphur isotopic interpretations of biosynthetic pathways; implications for biological signatures in the sulphur isotope record. Geobiology 1, 27–36.
Farquhar, J., Wing, B., 2003. Multiple sulfur isotopes and the evolution of the atmosphere. Earth Planet. Sci. Lett. 213, 1–13.
Fontaine, F.J., Rabinowicz, M., Boulègue, J., 2001. Permeability changes due to mineral diagenesis in fractured crust: implications for hydrothermal circulation at mid-ocean ridges. Earth Planet. Sci. Lett. 184, 407–425.
Fornari, D.J., Von Damm, K.L., Bryce, J.G., Cowen, J.P., Ferrini, V., Fundis, A., Lilley, M. D., Luther, III, G.W., Mullineaux, L.S., Perfit, M.R., Meana-Prado, F., Rubin, K.H., Seyfried, II, W.E., Shank, T.M., Soule, S.A., Tolstoy, M., White, S.M., 2012. The East Pacific Rise Between 9°N and 10°N Twenty-Five Years of Integrated, Multidisciplinary Oceanic Spreading Center Studies. Oceanogr. 25, 18–43.
Forrest, J., Newman, L., 1977. Silver-110 microgram sulfate analysis for the short time resolution of ambient levels of sulfur aerosol. Anal. Chem. 49, 1579–1584.
Frank, K.L., Rogers, D.R., Olins, H.C., Vidoudez, C., Girguis, P.R., 2013. Characterizing the distribution and rates of microbial sulfate reduction at Middle Valley hydrothermal vents. ISME. J. 7, 1391–1401.
Friedman, C.T., 1998. Analysis of stable sulfur isotopes and trace cobalt on sulfides from the TAG hydrothermal mound PhD Thesis. MIT and WHOI Joint Program.
Gemmell, J.B., Sharpe, R., 1998. Detailed sulfur-isotope investigation of the TAG hydrothermal mound and stockwork zone. In: Proceedings of the Ocean Drilling Program, Scientific Results 158, 71–84.
Giggenbach, W.F., 1974. Equilibria involving polysulfide ions in aqueous sulfide solutions up to 240°. Inorg. Chem. 13, 1724–1730.
Gittins, D.A., Desiage, P.A., Morrison, N., Rattray, J.E., Bhatnagar, S., Chakraborty, A., Zorz, J., Li, C., Horanszky, O., Cramm, M.A., Bisiach, F., Bennett, R., Webb, J., Macdonald, A., Fowler, M., Campbell, D.C., Hubert, C.R.J., 2022. Geological processes mediate a microbial dispersal loop in the deep biosphere. Sci. Adv. 8.
Glynn, S., Mills, R.A., Palmer, M.R., Pancost, R.D., Severmann, S., Boyce, A.J., 2006. The role of prokaryotes in supergene alteration of submarine hydrothermal sulfides. Earth Planet. Sci. Lett. 244, 170–185.
Golden, C.E., Webb, S.C., Sohn, R.A., 2003. Hydrothermal microearthquake swarms beneath active vents at Middle Valley, northern Juan de Fuca Ridge. J. Geophys. Res. 108, 2027.
Goodfellow, W.D., Blaise, B., 1988. Sulfide formation and hydrothermal alteration of hemipelagic sediment in Middle Valley, Northern Juan de Fuca Ridge. Canad. Mineral. 26, 675–696.
Goodfellow, W.D., Franklin, J.M., 1993. Geology, Mineralogy, and Chemistry of Sediment-Hosted Clastic Massive Sulfides in Shallow Cores, Middle Valley, Northern Juan de Fuca Ridge. Econ. Geol. 88, 2037–2068.
Goodfellow, W.D., Zierenberg, R.A., 1997. Genesis of Massive Sulfide Deposits at Sediment-Covered Spreading Centers. Rev. Econ. Geol.
Goordial, J., D'Angelo, T., Labonté, J.M., Poulton, N.J., Brown, J.M., Stepanauskas, R., Früh-Green, G.L., Orcutt, B.N., 2021. Microbial diversity and function in shallow subsurface sediment and oceanic lithosphere of the Atlantis Massif. mBio 12.
Halevy, I., Fike, D.A., Pasquier, B., R.N., Wenk, C.B., Turchyn, A.V., Johnston, D.T., Claypool, G.E., 2023. Sedimentary parameters control the sulfur isotope composition of marine pyrite. Science 382, 946–951.
Hannington, M.D., de Ronde, C.E.J., Peterson, S., 2005. Sea-Floor Tectonics and Submarine Hydrothermal Systems. Econ. Geol. 100th Anniversary Volume, 111–141.
Hannington, M.D., Jonasson, I.R., Herzig, P.M., Peterson, S., 1995. Physical and Chemical Processes of Seafloor Mineralization at Mid-Ocean Ridges. Geophys. Monogr. Ser. 91, 115–157.
Hannington, M.D., Scott, S.D., 1988. Mineralogy and geochemistry of a hydrothermal silica-sulfide-sulfate spire in the caldera of Axial Seamount, Juan De Fuca Ridge. Canad. Mineral. 26, 603–625.
Herzig, P.M., Petersen, S., Hannington, M.D., 1998. Geochemistry and sulfur-isotopic composition of the TAG hydrothermal mound, Mid-Atlantic Ridge, 26N. In: Proceedings of the Ocean Drilling Program, Scientific Results 158, pp. 47–67.
Holden, J., 2015. Processed Near-bottom Fluid Chemistry and Microbiology Data from the Juan de Fuca Spreading Center - Endeavour Segment acquired during R/V Atlantis expedition AT15-47 (2009). Marine Geoscience Data System.
Hughes, E.R., Waldeck, A.R., Moriarty, S.N., Jamieson, J.W., Martin, A.J., Scheuermann, P.P., Syverson, D.D., Seyfried, W.E., Reeves, E.P., Johnston, D.T., 2023. The influence of Submarine Hydrothermal Systems on Seawater Sulfate. Geochim. Cosmochim. Acta 344, 73–89.
Jaeschke, A., Eickmann, B., Lang, S.Q., Bernasconi, S.M., Strauss, H., Früh-Green, G.L., 2014. Biosignatures in chimney structures and sediment from the Loki's Castle low-temperature hydrothermal vent field at the Arctic Mid-Ocean Ridge. Extremophiles 18, 545–560.
Jamieson, J.W., Clague, D.A., Hannington, M.D., 2014. Hydrothermal sulfide accumulation along the Endeavour Segment, Juan de Fuca Ridge. Earth Planet. Sci. Lett. 395, 136–148.
Jamieson, J.W., Hannington, M.D., Clague, D.A., Kelley, D.S., Delaney, J.R., Holden, J.F., Tivey, M.K., Kimpe, L.E., 2013. Sulfide geochronology along the Endeavour Segment of the Juan de Fuca Ridge. Geochem. Geophys. Geosyst. 14, 2084–2099.
Jamieson, J.W., Hannington, M.D., Tivey, M.K., Hansteen, T., Williamson, N.M.B., Stewart, M., Fietzke, J., Butterfield, D., Frische, M., Allen, L., Cousens, B., Langer, J., 2016. Precipitation and Growth of Barite within Hydrothermal Vent Deposits from the Endeavour Segment, Juan de Fuca Ridge. Geochim. Cosmochim. Acta 173, 64–85.
Janecky, D.R., Seyfried II, W.E., 1984. Formation of massive sulfide deposits on oceanic ridge crests: Incremental reaction models for mixing between hydrothermal solutions and seawater. Geochim. Cosmochim. Acta 48, 2723–2738.
Johnston, D.T., 2011. Multiple sulfur isotopes and the evolution of Earth's surface sulfur cycle. Earth-Sci. Rev. 106, 161–183.
Johnston, D.T., Farquhar, J., Wing, B.A., Kaufman, A.J., Canfield, D.E., Habicht, K.S., 2005. Multiple sulfur isotope fractionations in biological systems: a case study with sulfate reducers and sulfur disproportionators. Am. J. Sci. 305, 645–660.
Johnston, D.T., Gill, B.C., Masterson, A., Beirne, E., Casciotti, K.L., Knapp, A.N., Berelson, W., 2014. Placing an upper limit on cryptic marine sulphur cycling. Nature 513, 530–533.
Jungbluth, S., Amend, J., Rappé, M., 2017. Metagenome sequencing and 98 microbial genomes from Juan de Fuca Ridge flank subsurface fluids. Sci. Data 4.
Kelley, D.S., Carbotte, S.M., Caress, D.W., Clague, D.A., Delaney, J.R., Gill, J.B., Hadaway, H., Holden, J.F., Hooft, E.E.E., Kellog, J.P., Lilley, M.D., Stoermer, M., Toomey, D., Weekly, R., Wilcock, W.S.D., 2012. Endeavour Segment of the Juan de Fuca Ridge: One of the most remarkable places on Earth. Oceanogr. 25, 44–61.
Kelley, D.S., Delaney, J.R., Juniper, S.K., 2014. Establishing a new era of submarine volcanic observatories: Cabling Axial Seamount and the Endeavour Segment of the Juan de Fuca Ridge. Mar. Geol. 325, 426–450.
Kelley, D.S., Delaney, J.R., Yoerger, D.R., 2001. Geology and venting characteristics of the Mothra hydrothermal field, Endeavour segment, Juan de Fuca Ridge. Geology 29, 959–962.
Kelley, D., Delaney, J., Yoerger, D., Caress, D., Clague, D., Denny, A., 2015. Processed Gridded (ESRI ASCII format) Bathymetry Data from the Juan de Fuca Endeavour Segment assembled as part of the JdF: Endeavour_Bathymetry Data Compilation. In: Interdisciplinary Earth Data Alliance (IEDA).
Klein, F., Humphris, S.E., Guo, W., Schubotz, F., Schwarzenbach, E.M., Orsi, W.D., 2015. Fluid mixing and the deep biosphere of a fossil Lost City-type hydrothermal system at the Iberia Margin. Proc. Natl. Acad. Sci. U. S. A. 112, 12036–12041.
Knott, R., Fouquet, Y., Honnorez, J., Petersen, S., Bohn, M., 1998. Petrology of hydrothermal mineralization: A vertical section through the TAG mound. In: Proceedings of the Ocean Drilling Program, Scientific Results 158, 5–26.
Kuznetsov, V., Cherkashev, G., Lein, A., Shilov, V., Maksimov, F., Arslanov, K., Stepanova, T., Baranova, N., Chernov, S., Tarasenko, D., 2006. ^{230}Th/U dating of massive sulfides from the Logatchev and Rainbow hydrothermal fields (Mid-Atlantic Ridge). Geochronometria 25, 51–55.
Labidi, J., Cartigny, P., Birck, J.L., Assayag, N., Bourrand, J.J., 2012. Determination of multiple sulfur isotopes in glasses: A reappraisal of the MORB δ^{34}S. Chem. Geol. 334, 189–198.
Labidi, J., Cartigny, P., Hamelin, C., Moreira, M., Dosso, L., 2014. Sulfur isotope budget (^{32}S, ^{33}S, ^{34}S and ^{36}S) in Pacific–Antarctic ridge basalts: A record of mantle source heterogeneity and hydrothermal sulfide assimilation. Geochim. Cosmochim. Acta 133, 47–67.
LaFlamme, C., Hollis, S.P., Jamieson, J.W., Fiorentini, M.L., 2018. Three-Dimensional Spatially Constrained Sulfur Isotopes Highlight Processes Controlling Sulfur Cycling in the Near Surface of the Iheya North Hydrothermal System, Okinawa Trough. Geochem. Geophys. Geosyst. 19, 2798–2812.
Lalou, C., Reyss, J.L., Brichet, E., Rona, P.A., Thompson, G., 1995. Hydrothermal activity on a 105-year scale at a slow-spreading ridge, TAG hydrothermal field, Mid-Atlantic Ridge 26°N. J. Geophys. Res. Solid Earth 100, 17855–17862.
Lein, A.Y., Ulyanova, N.V., Ulyanov, A.A., Cherkashov, G.A., Stepanova, T.V., 2001. Mineralogy and geochemistry of sulfide ores in ocean-floor hydrothermal fields associated with serpentinite protrusions. Russ. J. Earth Sci. 3, 371–393.
Lever, M.A., Rouxel, O., Alt, J.C., Shimizu, N., Ono, S., Coggon, W.C., Shanks III, W.C., Lapham, L., Elvert, M., Prieto-Mollar, X., Hinrichs, K., Inagaki, F., Teske, A., 2013. Evidence for Microbial Carbon and Sulfur Cycling in Deeply Buried Ridge Flank Basalt. Science 339, 1305–1308.

Lilley, M.D., Butterfield, D.A., Olsen, E.J., Lupton, J.E., Macko, S.A., McDuff, R.E., 1993. Anomalous CH_4 and NH_4^+ concentrations at an unsedimented mid-ocean ridge hydrothermal System. Nature 364, 45–47.
Machel, H.G., Krouse, H.R., Sassen, R., 1995. Products and distinguishing criteria of bacterial and thermochemical sulfate reduction. Appl. Geochem. 10, 373–389.
Masterson, A.L., 2016. Multiple Sulfur Isotope Applications in Diagenetic Models and Geochemical Proxy Records. Harvard University, Graduate School of Arts and Sciences. Doctoral Dissertation.
McDermott, J.M., Ono, S., Tivey, M.K., Seewald, J.S., Shanks III, W.C., Solow, A.R., 2015. Identification of sulfur sources and isotopic equilibria in submarine hot-springs using multiple sulfur isotopes. Geochim. Cosmochim. Acta 150, 169–187.
McDermott, J.M., Sylva, S.P., Ono, S., German, C.R., Seewald, J.S., 2020. Abiotic redox reactions in hydrothermal mixing zones: Decreased energy availability for the subsurface biosphere. Proc. Natl. Acad. Sci. U. S. A. 117, 20453–20461.
Monecke, T., Petersen, S., Hannington, M.D., M.d., 2014. Constraints on Water Depth of Massive Sulfide Formation: Evidence from Modern Seafloor Hydrothermal Systems in Arc-Related Settings. Econ. Geol. 109, 2079–2101.
Ohmoto, H., 1972. Systematics of carbon and sulfur isotopes in hydrothermal ore deposits. Econ. Geol. 67, 551–578.
Ohmoto, H., Mizukami, M., Drummond, S.E., Eldridge, C.S., Pisutha-Arnond, V., Lenagh, T.C., 1983. Chemical processes of Kuroko formation. Econ. Geol. Monogr. 5, 570–604.
Ono, S., Keller, N.S., Rouxel, O., Alt, J.C., 2012. Sulfur-33 constraints on the origin of secondary pyrite in altered oceanic basement. Geochim. Cosmochim. Acta 87, 323–340.
Ono, S., Shanks III, W.C., Rouxel, O.J., Rumble, D., 2007. S-33 constraints on the seawater sulfate contribution in modern seafloor hydrothermal vent sulfides. Geochim. Cosmochim. Acta 71, 1170–1182.
Ono, S., Wing, B.A., Johnston, D., Farquhar, J., Rumble, D., 2006. Mass-dependent fractionation of quadruple stable sulfur isotope system as a new tracer of sulfur biogeochemical cycles. Geochim. Cosmochim. Acta 70, 2238–2252.
Orcutt, B.N., Bach, W., Becker, K., Fisher, A.T., Hentscher, M., Toner, B.M., Wheat, C.G., Edwards, K.J., 2011. Colonization of subsurface microbial observatories deployed in young ocean crust. ISME. J. 5, 692–703.
Orcutt, B.N., Larowe, D.E., Biddle, J.F., Colwell, F.S., Glazer, B.T., Reese, B.K., Kirkpatrick, J.B., Lapham, L.L., Mills, H.J., Sylvan, J.B., Wankel, S.D., Wheat, C.G., 2013. Microbial activity in the marine deep biosphere: progress and prospects. Front. Microbiol. 4.
Perfit, M.R., Dorsey Wanless, V., Ridley, W.I., Klein, E.M., Smith, M.C., Goss, A.R., Hinds, J.S., Kutza, S.W., Fornari, D.J., 2012. Lava Geochemistry as a Probe into Crustal Formation at the East Pacific Rise. Oceanogr. 25, 89–93.
Peters, M., Strauss, H., Farquhar, J., Ockert, C., Eickmann, B., Jost, C.L., 2010. Sulfur cycling at the Mid-Atlantic Ridge: A multiple sulfur isotope approach. Chem. Geol. 269, 180–196.
Peters, M., Strauss, H., Petersen, S., Kummer, N.A., Thomazo, C., 2011. Hydrothermalism in the Tyrrhenian Sea: Inorganic and microbial sulfur cycling as revealed by geochemical and multiple sulfur isotope data. Chem. Geol. 280, 217–231.
Piercey, S.J., 2015. A semipermeable interface model for the genesis of subseafloor replacement-type volcanogenic massive sulfide (VMS) deposits. Econ. Geol. 110, 1655–1660.
Ran, B., Simoneit, B.R.T., 1994. Dissolved organic carbon in interstitial waters from sediments of Middle Valley. In: Proceedings of the Ocean Drilling Program, Scientific Results 139, 441–446.
Rouxel, O., Fouquet, Y., Ludden, J.N., 2004. Subsurface processes at the lucky strike hydrothermal field, Mid-Atlantic Ridge: Evidence from sulfur, selenium, and iron isotopes. Geochim. Cosmochim. Acta 68, 2295–2311.
Rouxel, O., Ono, S., Alt, J., Rumble, D., Ludden, J., 2008. Sulfur isotope evidence for microbial sulfate reduction in altered oceanic basalts at ODP Site 801. Earth Planet. Sci. Lett. 268, 110–123.
Ryan, W.B.F., Carbotte, S.M., Coplan, J., O'Hara, S., Melkonian, A., Arko, R., Weissel, R. A., Ferrini, V., Goodwillie, A., Nitsche, F., Bonczkowski, J., Zemsky, R., 2009. Global Multi-Resolution Topography (GMRT) synthesis data set. Geochem. Geophys. Geosyst.
Sakai, H., Casadevall, T.J., Moore, J.G., 1982. Chemistry and isotope ratios of sulfur in basalts and volcanic gases at Kilauea Volcano, Hawaii. Geochim. Cosmochim. Acta 46, 729–738.
Sakai, H., Des Marais, D.J., Ueda, A., Moore, J.G., 1984. Concentrations and isotope ratios of carbon, nitrogen and sulfur in ocean-floor basalts. Geochim. Cosmochim. Acta 48, 2433–2441.
Sánchez-Mora, D., Jamieson, J., Cannat, M., Escartin, J., Barreyre, T., 2022. Effects of Substrate Composition and Subsurface Fluid Pathways on the Geochemistry of Seafloor Hydrothermal Deposits at the Lucky Strike Vent Field, Mid-Atlantic Ridge. Geochem. Geophys. Geosyst. 23, 1–24.
Scholten, J.C., Lackschewitz, K.S., Marchig, V., Stoffers, P., Mangini, A., 2000. $^{230}Th/^{234}U$ and $^{231}Pa/^{235}U$ Disequilibria in massive sulfides from the Bent Hill area (Legs 139 and 169). In: Proceedings of the Ocean Drilling Program, Scientific Results 169, 1–15.
Schwarzenbach, E.M., Gill, B.C., Johnston, D., 2018. Unraveling multiple phases of sulfur cycling during the alteration of ancient ultramafic oceanic lithosphere. Geochim. Cosmochim. Acta 223, 279–299.
Seyfried, W.E., Seewald, J.S., Berndt, M.E., Ding, K., Foustoukos, D.I., 2003. Chemistry of hydrothermal vent fluids from the Main Endeavour Field, northern Juan de Fuca Ridge: Geochemical controls in the aftermath of June 1999 seismic events. J. Geophys. Res. 108, 2429.
Shanks III, W.C., 2001. Stable Isotopes in Seafloor Hydrothermal Systems: Vent fluids, hydrothermal deposits, hydrothermal alteration, and microbial processes. Rev. Mineral. Geochem.
Shanks III, W.C., Bischoff, J.L., 1980. Geochemistry, sulfur isotope composition, and accumulation rates of Red Sea geothermal deposits. Econ. Geol. 75, 445–459.
Shanks III, W.C., Bischoff, J.L., Rosenbauer, R.J., 1981. Seawater sulfate reduction and sulfur isotope fractionation in basaltic systems: Interaction of seawater with fayalite and magnetite at 200-350°C. Geochim. Cosmochim. Acta 45, 1997 1995.
Shanks III, W.C., Böhlke, J.K., Seal II, R.R., 1995. Stable Isotopes in Mid-Ocean Ridge Hydrothermal Systems: Interactions between Fluids, Minerals, and Organisms. Geophys. Monogr. 91, 194–221.
Stuart, F.M., Duckworth, R., Fallick, A.E., 1994a. Helium isotopes as tracers of trapped hydrothermal fluids in ocean-floor sulfides. Geology 22, 823–826.
Stuart, F.M., Duckworth, R., Turner, G., Schofield, P.F., 1994b. Helium and sulfur isotopes of sulfide minerals from Middle Valley, Northern Juan de Fuca Ridge. Proceedings of the Ocean Drilling Program, Scientific Results 139, 387–392.
Takai, K., Nakamura, K., Toki, T., Tsunogai, U., Miyazaki, M., Miyazaki, J., Hirayama, H., Nakagawa, S., Nunoura, T., Horikoshi, K., 2008. Cell proliferation at 122 degrees C and isotopically heavy CH_4 production by a hyperthermophilic methanogen under high-pressure cultivation. Proc. Natl. Acad. Sci. U. S. A. 105.
Thode, H.G., Monster, J., Dunford, H.B., 1961. Sulphur isotope geochemistry. Geochim. Cosmochim. Acta 25, 159–174.
Tostevin, R., Turchyn, A.V., Farquhar, J., Johnston, D.T., Eldridge, D.L., Bishop, J.K.B., McIlvin, M., 2014. Multiple sulfur isotope constraints on the modern sulfur cycle. Earth Planet. Sci. Lett. 396, 14–21.
Van Ark, E.M., Detrick, R.S., Canales, J.P., Carbotte, S.M., Harding, A.J., Kent, G.M., Nedimovic, M.R., Wilcock, W.S.D., Diebold, J.B., Babcock, J.M., 2007. Seismic structure of the Endeavour Segment, Juan de Fuca Ridge: Correlations with seismicity and hydrothermal activity. J. Geophys. Res. 112.
Von Damm, K.L., 2000. Chemistry of hydrothermal vent fluids from 9°–10°N, East Pacific Rise: "Time zero," the immediate posteruptive period. J. Geophys. Res. Solid Earth 105, 11203–11222.
Wilcock, W.S., Tolstoy, M., Waldhauser, F., Garcia, C., Tan, Y.J., Bohnenstiehl, D.R., Caplan-Auerbach, J., Dziak, R.P., Arnulf, A.F., Mann, M.E., 2016. Seismic constraints on caldera dynamics from the 2015 Axial Seamount Eruption. Science 354, 1395–1399.
Wu, N., Farquhar, J., Dottin III, J.W., Magalhaes, N., 2018. Sulfur isotope signatures of eucrites and diogenites. Geochim. Cosmochim. Acta 233, 1–13.
Yang, K., Scott, S.D., 1996. Possible contribution of a metal-rich magmatic fluid to a sea-floor hydrothermal system. Nature 383, 420–423.
Yang, K., Scott, S.D., 2002. Magmatic Degassing of Volatiles and Ore Metals into a Hydrothermal System on the Modern Sea Floor of the Eastern Manus Back-Arc Basin, Western Pacific. Econ. Geol. 97, 1079–1100.
You, C.F., Butterfield, D.A., Spivack, A.J., Gieskes, J.M., Gamo, T., Campbell, A.J., 1994. Boron and halide systematics in submarine hydrothermal systems—Effects of phase separation and sedimentary contributions. Earth Planet. Sci. Lett. 123, 227–238.
Yucel, M., Luther III, G.W., 2013. Temporal trends in vent fluid iron and sulfide chemistry following the 2005/2006 eruption at East Pacific Rise, 9°50'N. Geochem. Geophys. Geosyst. 14, 759.
Zeng, Z., Ma, Y., Chen, S., Selby, D., Wang, X., Yin, X., 2017. Sulfur and lead isotopic compositions of massive sulfides from deep-sea hydrothermal systems: Implications for ore genesis and fluid circulation. Ore Geol. Rev. 87, 155–171.
Zierenberg, R.A., 1994. Data report: Sulfur content of sediment and sulfur isotope values of sulfide and sulfate minerals from Middle Valley, Leg 139. Proceedings of the Ocean Drilling Program, Scientific Results 139, 739–748.
Zierenberg, R.A., Fouquet, Y., Miller, J., Party, S.S., 1998. The deep structure of a seafloor hydrothermal deposit. Nature 392, 485–488.
Zierenberg, R.A., Koski, R.A., Morton, J.L., Bouse, R.M., Shanks III, W.C., 1993. Genesis of Massive Sulfide Deposits on a Sediment-Covered Spreading Center, Escanaba Trough, Southern Gorda Ridge. Econ. Geol. 88, 2069–2098.